



**SIMULATION OF RADIATION ENVIRONMENT FOR
THE LARGE HADRON ELECTRON COLLIDER
DETECTOR**

Abdullah NAYAZ



T.C.
ULUDAĞ UNIVERSITY
INSTITUTE OF NATURAL AND APPLIED SCIENCE

**SIMULATION OF RADIATION ENVIRONMENT FOR THE LARGE HADRON
ELECTRON COLLIDER DETECTOR**

Abdullah NAYAZ

Asst. Prof. Zerrin KIRCA
(Supervisor)

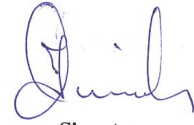
MSc Thesis
DEPARTMENT OF PHYSICS

BURSA–2017
All rights reserved

APPROVAL FOR THE THESIS

This work named " Simulation of Radiation Environment for the Large Hadron Electron Collider Detector" by Abdullah NAYAZ has been approved as a dissertation for the degree of **Master of Sciences in Physics** in the Department of Physics of Uludağ University by the below mentioned Examining Committee Members.

Supervisor: Asst. Prof. Zerrin KIRCA



Signature

Head: Asst. Prof. Zerrin KIRCA
Uludag University, Institute of
Natural and Applied Science,
Department of Physics



Signature

Member: Prof. Serkant Ali ÇETİN
Bilgi University, Faculty of En-
gineering and Natural Sciences,
Department of Energy Systems
Engineering



Signature

Member: Assoc. Prof. Cem Salih Ün
Uludag University, Institute of
Natural and Applied Science,
Department of Physics

Approved

Prof. Ali BAYRAM

Institute Director

28.12.2017

**I declare that this thesis follows the thesis preparation rules of Uludağ University
Institute of Natural and Applied Science. I hereby declare that;**

- all information in this document has been obtained in accordance with academic rules,
- all visual, audial and written information and results have been presented in academicethical rules,
- all citation and materials have been referenced as required by academic rules,
- all cited materials have been presented as reference,
- used sources and materials have not been altered,
- and this thesis has not been submitted for any degree or any other purposes.

.../.../2017

Signature

Abdullah Nayaz

ÖZET

Yüksek Lisans Tezi

BÜYÜK HADRON-ELEKTRON ÇARPIŞTRICISI ALGICINDA RADYASYON SEVİYESİ BENZETİŞİMİ

Abdullah NAYAZ

Uludağ Üniversitesi
Fen Bilimleri Enstitüsü
Fizik Anabilim Dalı

Danışman: Yrd. Doç. Dr. Zerrin KIRCA

CERN’de Büyük Hadron-Elektron Çarpıştırıcısı (BHeÇ), Büyük Hadron Çarpıştırıcısı’ndan (BHÇ) gelen 7 TeV’ lik protonların/iyonların, enerji geri dönüşüm hızlandırıcısında (ERL) üretilecek olan 60 GeV’lik elektronlar ile çarpışmasını inceleyecek üzere önerilen bir programdır. Geniş fizik programına, özellikle leptonlar ve kuark-gluon ile alakalı fizik hedeflerine sahip olan BHeÇ, BHÇ için tamamlayıcı bir proje olarak planlanmıştır ki bu hedefleri gerçekleştirmek için BHeÇ çalışma grubu tarafından çok amaçlı ve maksimum verimli bir algıç tasarlanmıştır. Yüksek enerjili çarpışan demetler nedeniyle algıçta yüksek bir ışınlık ve dolayısıyla yüksek bir radyasyon oluşması beklenmektedir. Algıçtaki radyasyon ortamının simülasyonu, projenin ömrü ve algıç hasarını tahmin etmek için büyük önem taşımaktadır.

Bu çalışmada FLUKA Monte Carlo kodunu kullanarak, LHeC algıcı için radyasyon ortamının benzetişimi yapılmıştır. Öncelikle, LHeC detektörünün geometrisi, BHeÇ’in kavramsal tasarım raporunda açıklandığı gibi, her alt algıç için gerekli radyasyon ve etkileşim uzunluğu değerleri dikkate alınarak FLUKA benzetişim programında tanımlanmıştır. Daha sonra ise, yeni benzetişim yapılan geometride, PYTHIA 6 olay üretim programı tarafından üretilen bir elektron-proton veri dosyası çalıştırılmıştır. LHeC algıcının tüm alt elemanlarında önemli radyasyon tahminleyicileri (parçacıkların dağılımı, Dose, NIEL vb.) öngörülmüştür. Sonuçlar iz sürücüde, özellikle ön bölgelerinde (forward regions), daha yoğun parçacık dağılımını göstermektedir. Ayrıca ön (forward) kalorimetrelere (FEC ve FHC) 7 TeV’lik proton demetleri nedeniyle daha yüksek radyasyona maruz kalmaktadır. Bunun yanında, algıç cevabı daha iyi incelenmesi için, izotropik olarak gönderilen proton olaylarının davranışı algıçta incelenmiştir.

Anahtar kelimeler: BHeÇ, BHeÇ algıcı, radyasyon seviyesi benzetişimi, algıç cevabı, FLUKA benzetişimi.

2017, xv + 50 Sayfa

ABSTRACT

MSc Thesis

SIMULATION OF RADIATION ENVIRONMENT FOR THE LARGE HADRON ELECTRON COLLIDER DETECTOR

Abdullah Nayaz

Uludağ University
Graduate School of Natural and Applied Science
Department of Physics

Supervisor: Asst. Prof. Zerrin KIRCA

The Large Hadron electron Collider (LHeC), a future project proposed at CERN, is designed to collide 60-140 GeV electron/positron beam accelerated in an Energy Recovery Linac (ERL) with the 7 TeV Proton or massive ion beam from existing Large Hadron Collider (LHC) machine. This is planned to be a complementary project for the LHC presenting an expanded range of physics goals especially those associated with leptons and quark-gluon. To accomplish these goals, a multi-purpose 4π detector with large acceptance Deep inelastic scattering (DIS) has been designed by the LHeC study group. A high luminosity and therefore an extreme radiation background is expected in the detector due to the high energy colliding beams. The simulation of this radiation is of great importance for estimating the detector damage and predictions over the lifetime of the project. This study presents the preliminary simulations of radiation environment for the LHeC detector using FLUKA Monte Carlo code. Firstly, the geometry of the LHeC detector was constructed in FLUKA using the LHeC detector baseline layout reported in LHeC CDR. The required radiation length X_0 and interaction length λ_I for each sub-system were taken into account while defining the new composite materials. Secondly, an electron-proton event data obtained by PYTHIA 6 event generator was run in the newly-built virtual geometry. The essential radiation estimators (Particle Fluence, Dose, NIEL) were predicted in all sub-systems of the LHeC detector. More intense particles fluence is foreseen in the tracker system, particularly in the forward regions. Forward Calorimeters (FEC and FHC) are also exposed to a higher radiation due to 7 TeV proton beams. Besides, for a better understanding of the detector response, the behavior of isotropically sent proton events in the detector is explored.

Key words: LHeC, LHeC Detector, detector response, radiation environment simulations, FLUKA simulations.

2017, xv + 50 Pages

ACKNOWLEDGEMENTS

I would like to express my greatest appreciation to my supervisor Asst. Prof. Zerrin KIRCA and Assoc. Prof. Ercan PİLİÇER for their guidance and all the support throughout the period of my study at the Uludağ University. They were never tired of answering my questions, and their patience and immense knowledge have always been a good motivation for my career goals.

I would like to thank the rest of my thesis examining committee Prof. Serkant Ali ÇETİN for his valuable discussions and revision of my thesis and also Assoc. Prof. Cem Salih ÜN for his useful comments and support.

I want to show my gratitude to Prof. İlhan TAPAN for his unforgettable classes and Prof. Emin N. ÖZMUTLU who patiently taught me the programming languages which helped me not only in my thesis but also in many other areas of my studies.

Special thanks for the constructive comments of Asst. Prof. Musa JUYA from Kabul Medical University whom his warm encouragements during the period of my study have been supportive.

I would like to thank all whom in one way or another contributed to the completion of this thesis. A great thank-you to Zafer ALTIN for helping me with the LATEX format to write my thesis, and to Nasir NIAZ, Bareera MARYAM, Faryal WASEER and Burçin AKSU who helped me in writing part. Also, a big thank-you to Ahmed SAAD for his encouragements and support during my studies.

Last but not least, I am very thankful to my family: my parents, brothers, and sisters. I would not stand where I am today without their continuous support.

Abdullah Nayaz

.../.../2017

CONTENTS

	Page
ÖZET	i
ABSTRACT	ii
ACKNOWLEDGEMENTS	iii
CONTENTS	iii
LIST OF ABBREVIATIONS	vi
LIST OF FIGURES	vii
LIST OF TABLES	ix
1. INTRODUCTION	1
2. THEORY	3
2.1. An Overview of High Energy Physics Detectors	3
2.2. The HERA Experiment	5
2.3. The Large Hadron Collider	6
2.4. Deep Inelastic Electron-Nucleon Scattering at the LHC	7
2.5. The Large Hadron Electron Collider	8
2.5.1. The LHeC Ring-Ring Option	9
2.5.2. The LHeC Linac-Ring Option	10
2.5.3. The Physics Programme	12
3. ANALYSIS	14
3.1. An Overview of LHeC Detector	14
3.2. Geometry of The LHeC Detector	15
3.2.1. Magnet system	15
3.2.2. Tracking detector	16
3.2.2.1. Pixel detector	17
3.2.2.2. Strip detector	18
3.2.2.3. The endcaps	19
3.2.2.4. Powering and cooling	21
3.2.3. Calorimetry	22
3.2.3.1. Electromagnetic calorimeter	22
3.2.3.2. Hadron calorimeter	24
3.2.4. Muon Detectors	26
3.3. The FLUKA Monte Carlo Code	27
4. SIMULATION RESULTS	29
4.1. Radiation Environment at the LHeC Detector	29
4.1.1. Particle Fluence	29
4.1.2. Energy Distribution and Ionizing Dose	34
4.1.3. Displacement Damage and NIEL	35

4.2. Detector Response	37
4.2.1. Particle Fluence	37
4.2.2. Energy Distribution	40
4.2.3. 1 MeV Neutron Equivalent Fluence	41
5. CONCLUSION	42
REFERENCES	43
CURRICULUM VITAE	50



LIST OF ABBREVIATIONS

Abbreviation	Description
LHC	Large Hadron Collider
LHeC	Large Hadron electron Collider
CDR	Conceptual Design Report
SM	Standard Mode
ERL	Energy Recovery Linac
DIS	Deep Inelastic Scattering
IP	Interaction Point
HERA	High Energy Ring Analge
ATLAS	A Toroidal LHC ApparatuS
CMS	Compact Muon Solenoid
ALICE	A Large Ion Collider Experiment
SPS	Super Proton Synchrotron
LR	Linac-Ring
RR	Ring-Ring
FCC	Future Circular Collider
EMC	Electromagnetic Calorimeter
HAC	Hadronic Calorimeter
CPT	Central Pixel Tracker
CST	Central Silicon Tracker
CFT	Central ForwardTracker
CBT	CentralBackward Tracker
FEC	Forward Electromagnetic Calorimeter
BEC	Backward Electromagnetic Calorimeter
FHC	Forward Hadronic Calorimeter
BHC	Backward Hadronic Calorimeter
DT	Drift Tubes
CST	Cathode Strip Chambers
RPC	Resistive Plate Chambers
NIEL	Non-Ionizing Energy Loss

LIST OF FIGURES

	Page
Figure 2.1. A hermetic HEP detector layout. Front view (right), side view (left). . .	4
Figure 2.2. The HERA experiment at DESY, Germany.	6
Figure 2.3. The overview of CERN’s accelerator complex.	7
Figure 2.4. Schematic view of the CERN’s accelerator complex. The LHeC location is near to ALIC (red line).	9
Figure 2.5. Schematic view of the LHeC RR option: The LEP tunnel now used for the LHC (grey/red) and three bypasses of ATLAS, CMS, and LHCb (blue) (Keil 1997).	10
Figure 2.6. Schematic layout of the LHeC ERL.	11
Figure 2.7. Key results of the exploration of the TeV scale colliders beginning by the LHC (top), and complementing by the LHeC (bottom left) and IL-C/CLIC e^-/e^+ colliders (Fernandez et al. 2012).	13
Figure 2.8. Kinematic regions in Bjorken- x and momentum transfers Q^2 for the H1 and ZEUS experiments at HERA and the LHeC (Dainton et al. 2006). .	13
Figure 3.1. Schematic $r - z$ view of the detector design for the Linac-Ring option. .	14
Figure 3.2. Te cryostat of the LHeC magnet system.	16
Figure 3.3. The $r - z$ view of Tracker detectors and Electromagnetic-Calorimeter for the LHeC baseline layout.	17
Figure 3.4. The exploded view of a barrel pixel for ATLAS detector full module (Alam et al. 1998).	18
Figure 3.5. A layout of a silicon strip used in the CMS Tracker (Kaußen 2008). . .	19
Figure 3.6. A layout of the 2-in-1 strip sensor design used in the CMS tracker module.	19
Figure 3.7. A fully assembled end-cap of CMS (Widl 2008).	20
Figure 3.8. The mechanics layout designed for the CMS inner tracker.	21
Figure 3.9. $x - y$ and $r - z$ view of the LHeC calorimetry, EMC (green) and HAC (pink).	22
Figure 3.10. Accordion structure of ATLAS LAr Calorimeter with a longitudinal view of its one cell.	23
Figure 3.11. The 3D view of the ATLAS EM barrel detector, displaying the accordion structure.	24
Figure 3.12. An $r - z$ view of HAC, FHC1-FHC3, BHC1-BHC3 of the LHeC detector.	25
Figure 3.13. A full view of the baseline detector in the $r - z$ plane with all components shown. The dimensions are $\approx 14 \text{ m} \times 9 \text{ m}$	27
Figure 3.14. An artist 3D view of the projective arrangement of the barrel layer muon chambers (left). A schematic view of the cross section of one of the chambers (right) (Fernandez et al. 2012).	27
Figure 3.15. The pseudorapidity of particles in ep data generated by PYTHIA 6. . .	28
Figure 3.16. The momentum of particles in ep data generated by PYTHIA 6. . . .	28

Figure 4.1. The fluence of all charged particles [particles/cm ² /sec] in the LHeC detector.	30
Figure 4.2. The distribution of hadrons with energy greater than 20 MeV.	30
Figure 4.3. The neutrons fluence in the LHeC detector.	31
Figure 4.4. The protons fluence in the LHeC detector.	32
Figure 4.5. The photons fluence in the LHeC detector.	32
Figure 4.6. The pions fluence in the LHeC detector.	33
Figure 4.7. The muons fluence in the LHeC detector.	33
Figure 4.8. Energy distribution in the LHeC detector.	34
Figure 4.9. Dose distribution in the LHeC detector.	35
Figure 4.10. Displacement damage in Silicon for neutrons, pions, protons and electrons.	36
Figure 4.11. 1 MeV neutron equivalent fluence in the LHeC detector.	36
Figure 4.12. FLUKA prediction for the non-ionizing energy loss (GeV), in the LHeC detector.	37
Figure 4.13. The distribution of all particles [particles/cm ² /sec] in the LHeC detector as a result of 7 TeV proton events.	38
Figure 4.14. The neutrons fluence in the LHeC detector as a result of 7 TeV proton events.	38
Figure 4.15. The fluence of muons at the LHeC detector as a result of 7 TeV proton events.	39
Figure 4.16. The distribution of hadrons with energy greater than 20 MeV [hadrons>20 MeV/cm ² /sec] in the LHeC detector as a result of 7 TeV proton events.	40
Figure 4.17. The distribution of energy [GeV/cm ³ /sec] in the LHeC detector as a result of 7 TeV proton events.	40
Figure 4.18. 1 MeV neutron equivalent flux in the LHeC detector as a result of 7 TeV proton events.	41

LIST OF TABLES

	Page
Table 2.1. Main LHeC Ring-Ring option parameters.	10
Table 2.2. Parameters for LHeC linac option, 60 GeV ERL and 140 GeV pulsed. . .	11
Table 3.1. Dimensions of the LHeC magnet system.	16
Table 3.2. Summary of the Central Pixel and Central Strip Tracker (CPT/CST). . .	18
Table 3.3. Summary of the Central Forward and Backward Trackers (CFT/CBT). . .	20
Table 3.4. Summary of the Forward and Backward Silicon Trackers (FST/BST). . .	21
Table 3.5. The details of the LHeC electromagnetic calorimeter.	23
Table 3.6. Summary of the hadronic calorimeter barrel part dimensions.	25
Table 3.7. Summary of the FHC and BHC dimensions.	25

1. INTRODUCTION

The fundamental structures of matter and the forces between them are the main topics of High Energy Physics (HEP) which is also known as Particle Physics. In the history of Particle Physics, many basic building blocks were accepted as the fundamental constituents of matter. For instance, at the end of the 19th century, atoms were believed as the fundamental blocks of matter which can not be further subdivided. However, later on, the internal structure of atom was discovered and the electron, proton, and neutron became the elementary particles. The most updated knowledge about the issue is presented by Standard Model (SM) (Wiese 2010), which has the most successful explanation of the elementary particles and forces between them. According to this model, leptons and quarks are grouped into three families of 2+2 each. These particles are governed by four forces: the strong force, the weak force, the electromagnetic force and the gravitational force. These forces are mediated by gauge bosons. Although the SM has been successful in explaining the structure of the universe (Egana-Ugrinovic 2016), still there have been some drawbacks in describing the dark matter, dark energy, neutrino masses, etc.

A deeper exploration of the structure of matter and the universe requires large particle accelerators to give more energy to the colliding particle beams. The Large Hadron Collider (LHC) at CERN, as briefly outlined in section 2.3, has been the largest high energy experimental center in the world until now which can reach ≈ 14 TeV center-of-mass energy (Evans and Bryant 2008, CERN 2017).

As part of the LHC, the Large Hadron Electron Collider (LHeC) is also proposed to be one of the High Energy Physics experiments at CERN. It has been planned to collide 7 TeV proton or heavy ion beams from existing LHC machine with 60 – 140 GeV electron beam accelerated by Energy Recovery Linac (ERL).

Before LHeC, HERA at DESY, Germany, was known as the biggest electron-proton collider ever built which pushed the Deep Inelastic Scattering (DIS) energy to reach the Fermi scale. HERA which is still known as the first e-p collider ever, was designed for the collision of the electron and proton beams with energies of 30 GeV and 1 TeV respectively. The beams were accelerated in a 6 km circumference tunnel. According to the

achievements considered for HERA, it reached the luminosity of $L \approx 10^{31} \text{cm}^{-2} \text{s}^{-1}$ and continued its operation until 2007.

Since the accelerator ring of the LHC for proton/ion beam was already in operation, to make better use of it, the idea of having an electron proton (ep) collider (the LHeC) was introduced. In the middle of nineties, a study was performed suggesting two options for the electron accelerator part of LHeC; a new lepton ring in the LHC tunnel, Ring-Ring (RR) option, and an electron linear accelerator, Linac-Ring (LR) option.

The LHeC has a wide range of physics programme which is crucial in expanding the capabilities of the LHC. It brings the possibilities of discovery for physics beyond the SM with high precision deep inelastic scattering measurements. A considerable radiation environment is created in the detector due to the high luminosity and energy during the collisions. The radiations, higher than minimum bias background, start to influence the detector and may damage semiconductor devices. It also may lead to saturation of the detector or its occupancies beyond the tolerable level. The simulation of radiation environment for the detector is necessary to predict the behaviour of the detector system and its performance over the lifetime of the project.

In this study, the geometry of LHeC detector is built in FLUKA (FLUKA 2017) according to LHeC Conceptual Design Report CDR (Fernandez et al. 2012). The material of each component is defined newly from the composite of all materials used in the respective part according to their X/X_0 . As a result, the detector response and simulation of radiation environment for the LHeC detector, such as the dose distribution and the fluences of different particles (charged particles, protons, muons etc.) are presented. For detector response studies, events of protons with 7 TeV energy were sent isotropically from the interaction point of the detector. While an electron-proton collision data, generated by Pythia 6 (Pythia 2013), is used for simulation of radiation environment. The significant radiation estimators are then presented.

In the following sections, some HEP Experiments like HERA and LHC are shortly recalled. The details of the LHeC project, its Physics goals and the two possible options of the project are reviewed. The LHeC detector and the parameters used in the FLUKA simulation are explained in chapter 3. Finally, chapter 4 presents the simulation results for the radiation environment and the detector response.

2. THEORY

2.1. An Overview of High Energy Physics Detectors

Exploration of the fundamental constituents of matter, as mentioned above, requires large particle colliders like LHC to accelerate particles beams and bring them into collision at the highest energy possible. The collision can take place either between two accelerated particle beams (head-on collision) or between the colliding beam and a fixed target. After the crash, new-generated particles and their interactions are investigated in the detectors built around the interaction point (IP). Many detection principles are being used in High Energy Physics. Using gaseous detectors, solid-state detectors and scintillator detectors are the most common methods. The gaseous detectors are based on the ionization (electron-ion pair production) that take place by a charged particle as it passes through matter. While the solid-state detectors utilize semiconductor materials such as silicon or germanium crystal. In scintillators, photons are released when an electron returns to its ground state (excitation mechanism). Scintillations are then monitored by photomultiplier tubes which convert them to electrical signals (Gruppen and Shwartz 2008). A detector at particle colliders based on the physics goals of the experiment can use different technologies mentioned above.

A typical detector used on a collider includes vertex detector, tracker, calorimeter, and muon detector. A schematic view of a typical High Energy Physics detector system is illustrated in Figure 2.1 showing all sub-detectors (Moser 2009). For the LHeC detector layout, see Figure 3.1.

Tracker, with a larger radii $\approx 1-2$ m, is positioned after the vertex layers. The main task of tracking detector is to monitor the path of the particles which are curved under the magnetic field provided by the magnet system of the detector. The measurements of the curvature by the tracker allow us to determine the momentum of the particles. Tracker also exploits silicon detectors like strip sensors and gaseous detectors (Green 2005, Kayl 2010).

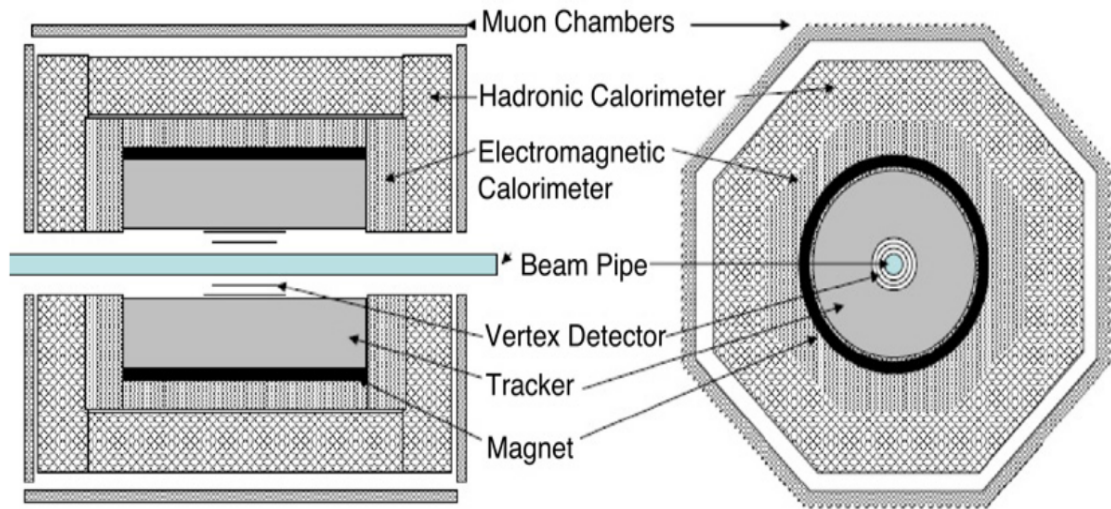


Figure 2.1. A hermetic HEP detector layout. Front view (right), side view (left).

Calorimetry is designed to measure the energy of the incident particles generated in the strong and electromagnetic interactions in the detector. The measurement is done by entirely absorbing the incident particles and then converting their energies to detectable light or electronic signal. There is less disturbance for particles that traverse tracking detectors. However, the interaction and the deposited energy by the incident particles are maximum in the calorimeter detectors where the electromagnetic and hadronic showers take place. Calorimetry has electromagnetic and hadronic parts specialized to deal with electromagnetic and hadronic showers respectively. The particles involved in the electromagnetic shower are electrons, positrons, and photons, while hadrons (particles made of quarks) are produced in hadronic shower with a comparatively longer range (Fabjan and Gianotti 2003). This extensive range requires a large enough region to contain the entire hadronic showers. From the point of construction technique, calorimeter detectors are classified into homogeneous and sampling calorimeters. In the homogeneous calorimeter, a single medium (e.g. $PbWO_4$ or BGO crystals) serves as both absorber and the active material. Sampling calorimeters, on the other hand, are built of alternating layers (e.g. Pb and LAr) for absorption and signal generation.

Muons (Gorringe and Hertzog 2015), unlike the most of other particles, can travel large distances even without any interaction. The muon detectors are, therefore, placed in the

very outer region where no other particles like hadrons or electrons can reach. The most common interaction mechanism for muons is ionization by which they can be detected easily in the outermost region. The detection process is performed mainly by gaseous and scintillation detectors. By passing through the gas volume of the detector, the incident muons produce electron-ion pairs whose absorptions in the anode and cathode induce the detectable electrical signal. Scintillators are also used in some cases for accurate time measurement of muon tracks and positions. The magnetic field in the muon detector helps us for the analyses of muon's momentum. More information about the principles of muon detectors can be found in (Paolucci 2006, Arai et al. 2008).

2.2. The HERA Experiment

High Energy Ring Anlage (HERA), the very first electron-proton collider, was built at DESY (German Electron Synchrotron) in Hamburg city of Germany in 1992 (Klein and Yoshida 2008). HERA (HERA 2006) was known as the only experimental center in the world, in which e^-/e^+ and proton beams were accelerated separately in a 6.3-Km-long tunnel located deep below the ground, to reach the required amount of energy ($E_e \approx 27$ GeV and $E_p \approx 920$ GeV). The beams were then brought to a head-on collision. The H1 and ZEUS detectors were designed to investigate high energy ep interactions with nearly 4π acceptance and a solenoidal field of 1.2 T and 1.43 T, respectively. The first phase of operation at HERA, "HERA I" was taken place from 1992 through 2000, while after the upgrade to achieve a higher luminosity (almost by a factor of four of HERA I), the second data-taking phase "HERA II" was begun in 2003. The research operation at HERA was continued until the end of June 2007. The experiences gained at this experiment played a crucial role in design and installation of the LHC at CERN (Amaldi 2015, CERN 2017). Figure 2.2 shows a part of proton and electron beam tunnels at HERA project.



Figure 2.2. The HERA experiment at DESY, Germany.

2.3. The Large Hadron Collider

The Large Hadron Collider (LHC), the world's largest particle accelerator until now, is located at the European Organization for Nuclear Research (CERN) close to the border of Switzerland and France, where a two-ring superconducting proton-proton collider is installed in a 27 km tunnel buried 50 – 150 m below the ground surface to investigate the resulting particle interactions. A magnetic field of 8.3 T, provided by the Superconducting dipole magnets, is required to keep the protons or ions in orbit during the acceleration. The superconducting magnets are cooled using liquid helium at a temperature of 1.9 K. The proton or ion beams accelerated in the opposite directions, nearly at the speed of light, are collided at four different experiments (ALICE, ATLAS, CMS, and LHCb) along the ring.

Two general purpose experiments, A Toroidal LHC ApparatuS (ATLAS) and the Compact Muon Solenoid (CMS), focus on understanding the nature of electroweak symmetry breaking and Higgs boson (The CMS Collaboration et al. 2008, Plehn 2012). The Large Hadron Collider beauty experiment (LHCb) is dedicated to B Physics and A Large Ion Collider Experiment (ALICE) investigates the physics of heavy ion collisions. There is also the TOTal cross section, Elastic scattering, and diffraction dissociation Measurements (TOTEM) experiment.

The LHC is designed to provide collisions with high luminosity of $\approx 10^{34} \text{cm}^{-2} \text{s}^{-1}$ and a center of mass energy of $\sqrt{s} = 14 \text{TeV}$. Protons, obtained from hydrogen atoms, are first injected into some smaller accelerators; Linac2, PS Booster, Proton Synchrotron and

Super Proton Synchrotron (SPS), where proton beams are given the energies of 50 MeV, 1.4, 25 and 450 GeV by each accelerator respectively. When the proton beams gain the required energy, they are injected into the LHC where they are accelerated to their final energy level.

The main purpose of the LHC is to understand the nature of electroweak symmetry breaking and to explore potential manifestations of new physics phenomena beyond the Standard Model (BSM).

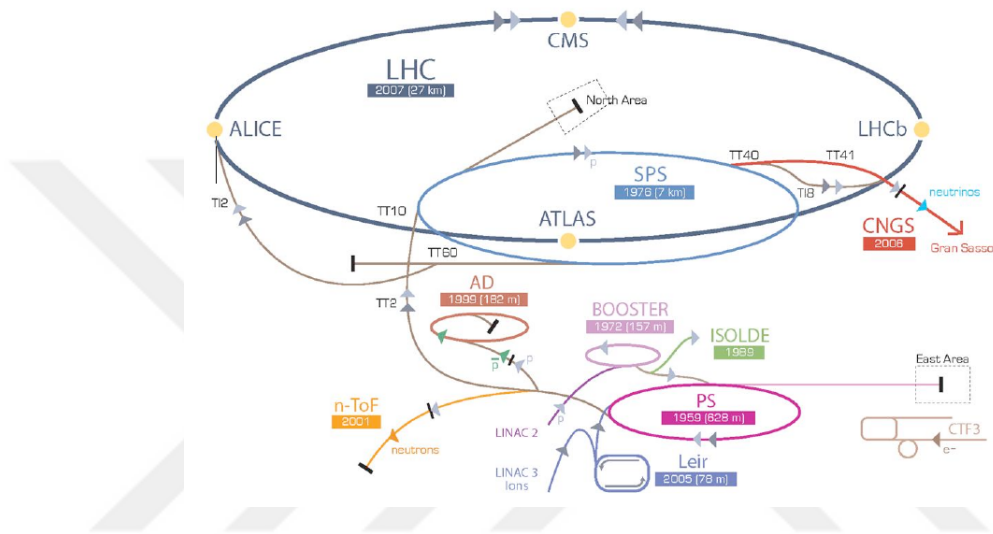


Figure 2.3. The overview of CERN’s accelerator complex.

2.4. Deep Inelastic Electron-Nucleon Scattering at the LHC

The electron-proton (ep) scattering at the LHC was presented at the first ECFA-CERN workshop on the feasibility of Hadron Colliders in the Large Electron-Positron Collider (LEP) Tunnel in March 1984, where the physics of electron-proton (ep) collision was studied (Altarelli et al. 1984) in the range of center-of-mass energies between $\sqrt{s} \approx 0.3$ TeV (HERA) and $\sqrt{s} \approx 1 - 2$ TeV. The later energy was considered if the e^-/e^+ beam from LEP collided with the proton beam of the LHC. Later on, since the 7 TeV proton or ion beams of the LHC ring were already in implementation, it was reasonable to think of exploiting one of these beams as a part of new (ep) or electron-ion (eA) collider- the Large Hadron electron Collider (LHeC).

In the middle of nineties upon the request of the CERN Scientific Policy Committee

(SPC), a study on electron-proton ring option with an estimated luminosity of $L \approx 10^{32} \text{cm}^{-2} \text{s}^{-1}$ was presented (Keil 1997). Finally, the more detailed study on Deep Inelastic electron-nucleon Scattering at the LHC was performed (Dainton et al. 2006), demonstrating for the first time that the luminosity of $L \approx 10^{33} \text{cm}^{-2} \text{s}^{-1}$ could be achieved. It suggested a 70 GeV e^-/e^+ beam in the LHC tunnel to collide with one of the LHC hadron beams operating simultaneously.

2.5. The Large Hadron Electron Collider

The Large Hadron Electron Collider (LHeC), a future project proposed at CERN, has been designed to collide 7 TeV proton or heavy ion beam from existing Large Hadron Collider (LHC) machine with 60 – 140 GeV electron beam accelerated by Energy Recovery Linac (ERL). The performances set for the LHeC, lead it to be the first experiment studying deep inelastic lepton-hadron (ep , eD and eA) scattering at the TeV energy scale for momentum transfers Q^2 beyond 106GeV^2 and for Bjorken x down to 10^{-6} . Providing a high luminosity of $L = 10^{33} \text{cm}^{-2} \text{s}^{-1}$ and a center of mass energy of $\sqrt{s} = 1,4 \text{TeV}$, the LHeC therefore, represents an excellent opportunity of exploring a new regime of energy and luminosity for DIS and the determination of hadron structure, as studied in QCD. This high precision lepton-hadron collision brings in a crucial accuracy in the physics goals of the LHC and extends its capabilities, especially in the matter of exploration of hadron structure (Dainton et al. 2006, Brüning 2013). The luminosity achievable in the LHeC is 100 times higher as compared to the previous ep collider, HERA, while it is four times higher in case of the center of mass energy (Cruz-Alaniz et al. 2015).

The LHeC Conceptual Design Report (CDR), published in 2012, was developed under the auspices of CERN, European Committee for Future Accelerators (ECFA), and Nuclear Physics European Collaboration Committee (NuPECC) (Körner 2017). It explores two distinctly different options for the LHeC; a new lepton ring in the LHC tunnel (Ring-Ring option) and an electron linac along with the LHC (Linac-Ring option). The Linac-Ring option was then preferred for implementation due to economic reasons as well as for conservation of the LHC tunnel. The complex of both options is given in Figure 2.5.1.

In consideration of the requirements of the LHeC experiment, a hermetic and asymmetric 4π detector has been designed for both Linac-Ring (LR) and Ring-Ring (RR) options by the LHeC study group, as documented in the CDR (Fernandez et al. 2012). The LHeC detector baseline layout, from center to the outer layer, consists of tracker detectors (central, forward and backward tracker), calorimeters (electromagnetic and hadronic calorimeters), and the muon system. A strong solenoid (3.5 T) separates the electromagnetic and hadronic calorimeters. See Figure 3.1. More details about the LHeC detector can be found in the section 3.

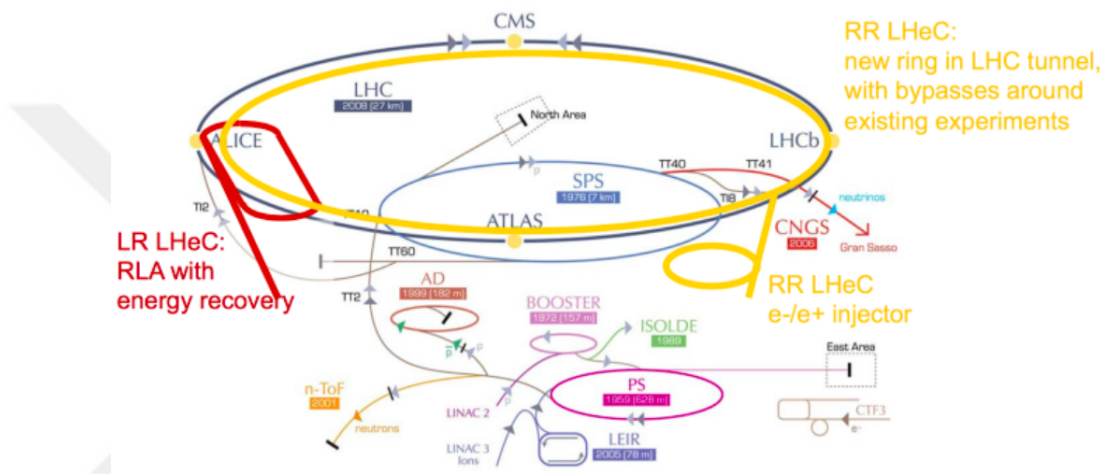


Figure 2.4. Schematic view of the CERN’s accelerator complex. The LHeC location is near to ALICE (red line).

2.5.1. The LHeC Ring-Ring Option

When the LHC project (Verdier 1991) at CERN was intended to be installed in the LEP tunnel, the overlap in the exploitation of LEP and LHC brought up the idea of an ep Ring-Ring collider. However, later on, it was decided to install the LHC in the LEP tunnel after complete removal of the LEP machine, an additional lepton ring was proposed to be built on the top of the LHC tunnel (Lehrach 2012) with three bypasses towards the outside of the ring in isolated tunnels each of which is 1.3 km long (Klein 2011). See Figure 2.5. This layout could benefit from known technologies and experiences gained at HERA and LEP. Some of the LHeC Ring-Ring parameters are summarized in Table 2.1. For further information about RR configuration refer to (Keil 1997, Fernandez et al. 2012, Burkhardt

2012).

Table 2.1. Main LHeC Ring-Ring option parameters.

Parameter	Value
Electron beam energy	60 GeV
e^+, e^- intensity per bunch	2×10^{10}
Total e^+, e^- beam current	100 mA
# bunches	2808
ep Luminosity (HL-layout)	$1.3 \times 10^{33} \text{ cm}^{-2} \text{ s}^{-1}$
Total wall plug power	100 MW
Transverse normalized emittance $\epsilon_{Nx,y}$	0.59, 0.29 mm

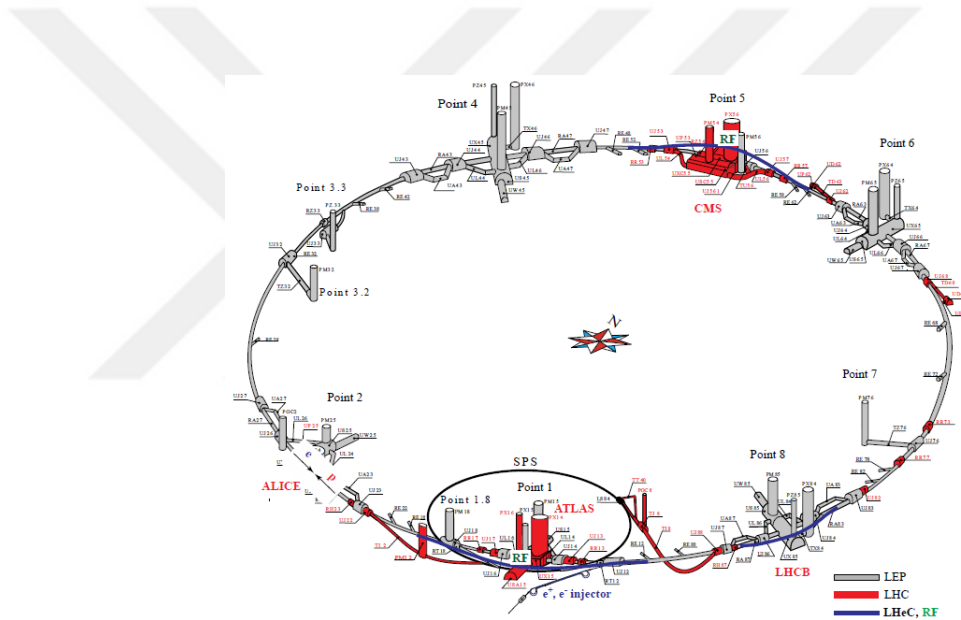


Figure 2.5. Schematic view of the LHeC RR option: The LEP tunnel now used for the LHC (grey/red) and three bypasses of ATLAS, CMS, and LHCb (blue) (Keil 1997).

2.5.2. The LHeC Linac-Ring Option

As outlined in the previous sections, the LHeC project can also be visualized as a Linac-Ring collider, which requires a new Linear accelerator (Linac) for the electron (or positron) beam. The linac, based on superconducting (SC) radio frequency (RF) technology (Nasiri et al. 2016), accelerates the electron (or positron) beams to 60 – 140 GeV and collides

them with the 7 TeV proton beams circulating in the current LHC tunnel. Of the several options studied for the linear accelerator (pulsed, recirculating and Energy Recovery Linac configurations), a recirculating 60 GeV Energy Recovery Linac (ERL) (Zimmermann 2013, Bogacz et al. 2015) has been chosen for accelerating the e/e^+ beams. The 60 GeV ERL version consists of two superconducting RF sections 1 Km each and two return arcs that house magnets for three passages at different energies. Since each linac section provides an energy gain of 10 GeV, the machine requires total three revolutions to reach the required energy of 60 GeV (Zimmermann 2012, Brüning 2013). Figure 2.6 shows a schematic layout of the 60 GeV ERL option including the dimensions. The LHeC baseline linac parameters for the 60 GeV ERL and 140 GeV pulsed option are summarized in Table 2.2 (Brüning 2013).

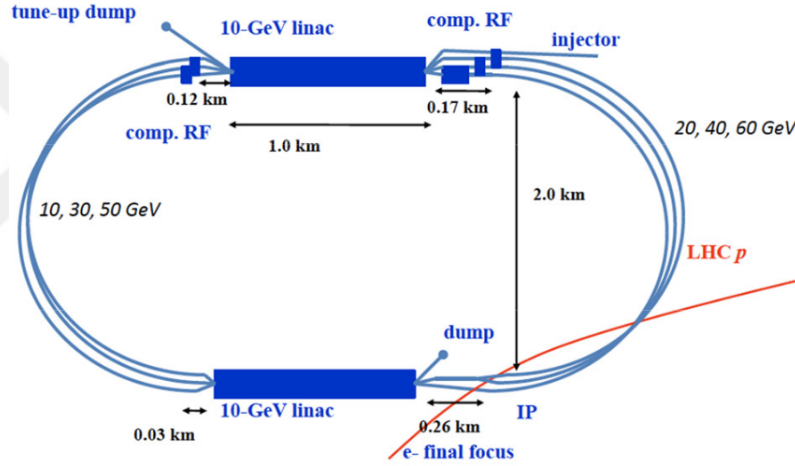


Figure 2.6. Schematic layout of the LHeC ERL.

Table 2.2. Parameters for LHeC linac option, 60 GeV ERL and 140 GeV pulsed.

Operation mode	CW	Pulsed
Beam Energy [GeV]	60	140
Peak Luminosity [$cm^{-2}s^{-1}$]	10^{33}	4×10^{31}
Cavity gradient [MV/m]	20	32
Cavity Q_0	2.5×10^{10}	2.5×10^{10}
RF length [km]	2	7.9
Total length [km]	9	7.9
Beam current [mA]	6.4	0.27

2.5.3. The Physics Programme

The inclusive physics programme of the LHeC project is documented extensively in the LHeC CDR. It has been organized in three general sections; New Physics at Large Scales, QCD and Electroweak Physics, Low x and Nuclear Physics. The intense proton or ion beam of the LHC along with the new e/e^+ beam from ERL can provide a high luminosity of $\approx 10^{31} \text{ cm}^{-2} \text{ s}^{-1}$ which is around 100 times larger than that achieved at HERA. It can yield a center of mass energy of almost 2 TeV (Cruz-Alaniz et al. 2015) and would probe distance scales of the order of 10^{-20} m (Dainton et al. 2006). With high luminosity and low Bjorken- x , the new TeV scale ep and eA energy frontier collider pursue the new aspects of physics beyond the Standard Model (BSM). The LHeC can completely unfold the partonic content of the proton and give us the knowledge about quantum chromodynamic phenomena and hadron or nucleus structure (the Quark-Gluon distributions). Since HERA was not designed to collide electrons with deuterons or ions, a good opportunity for exploration of the electron-deuteron and electron-ion scattering (Rossi 2016) with high Q^2 and low x is provided by the proton/ion beam of the LHC ring. The phase space which will be extended by the LHeC is shown in Figure 2.8.

A TeV-energy-scale lepton hadron collider like the LHeC, provides us with the chances of investigation into new areas of physics especially those associated with leptons and quark-gluon described by QCD (Perez and Rizvi 2013). LHeC data could separately constrain all of the quark flavors for the first time in a single experiment.

When exploring new physics, the electron-quark vertex requires precision study considering the pure-lepton and pure-strongly-interacting vertices. The LHeC has a unique potential for precision electroweak physics reaching high scales and effective couplings, and provides a good sensitivity to new leptons or particles with both lepton and baryon quantum numbers. Therefore, it can be an excellent complement for the LHC discovery potential-especially for physics BSM (Newman 2009, Staśto 2011).

The TeV Scale [2010-2035..]

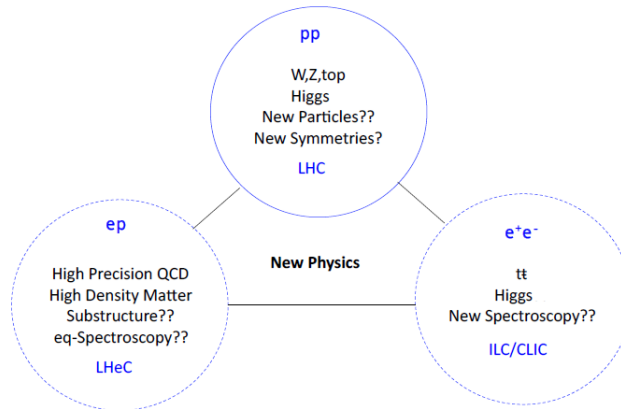


Figure 2.7. Key results of the exploration of the TeV scale colliders beginning by the LHC (top), and complementing by the LHeC (bottom left) and ILC/CLIC e^-/e^+ colliders (Fernandez et al. 2012).

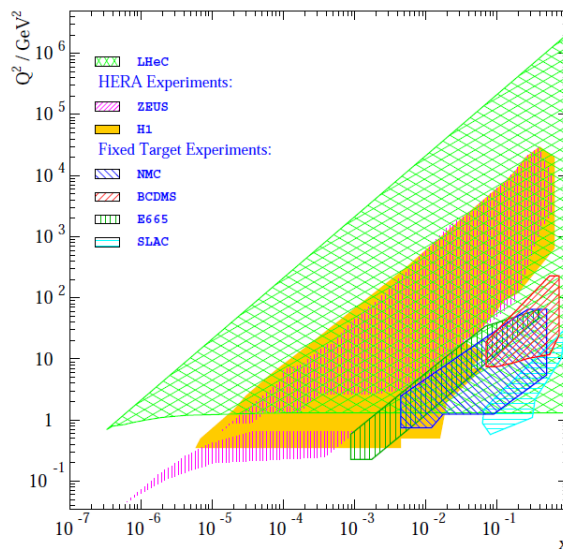


Figure 2.8. Kinematic regions in Bjorken-x and momentum transfers Q^2 for the H1 and ZEUS experiments at HERA and the LHeC (Dainton et al. 2006).

3. ANALYSIS

3.1. An Overview of LHeC Detector

The LHeC detector baseline layout, designed by LHeC study group, presents a hermetic and asymmetric detector with a high precision and 4π acceptance (Polini et al. 2012, Kostka et al. 2013). The detector design has been presented for both Linac-Ring and Ring-Ring options, however, due to some reasons like being less intrusive for LHC running and being synergic with Future Circular Collider (FCC), the LR design, as shown in Figure 3.1, has been preferred as the baseline layout. Therefore, this simulation uses the details and characteristics of the LR detector baseline layout reported in the CDR (Fernandez et al. 2012).

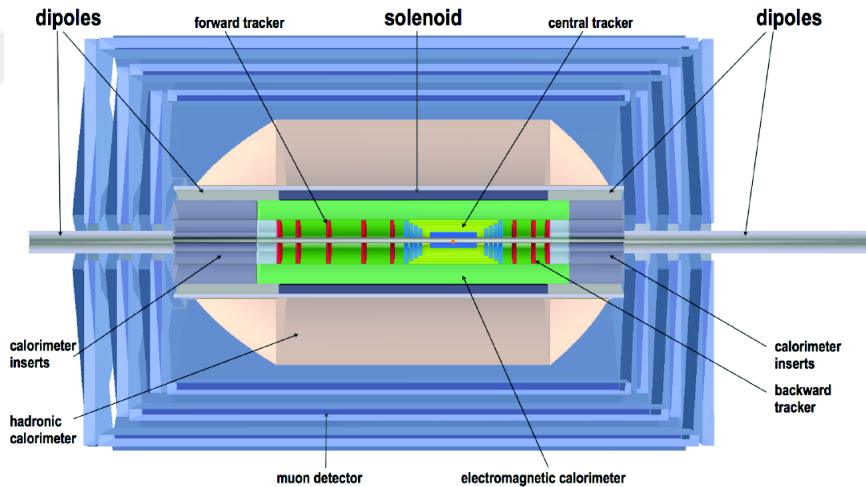


Figure 3.1. Schematic $r - z$ view of the detector design for the Linac-Ring option.

The LHeC detector, as depicted in Figure 3.1, consists of a central tracker extended with forward and backward tracking detectors surrounded by the electromagnetic calorimeter which is separated by a strong solenoid (3.5 Tesla) from the hadronic calorimeter. The detector, finally, covered by the muon system. The dimensions of the main LHeC detector are $14\text{ m} \times 9\text{ m}$ which are much smaller than the CMS or ATLAS (Polini et al. 2012).

This chapter gives a short description about geometry of the LHeC detector with some details of each sub-detector presented by the LHeC study group (Fernandez et al. 2012). Based on this information, the FLUKA simulations are then presented. Some required information regarding material composition, which is not mentioned in the CDR, are taken from CMS and ATLAS designs. This is based on the similarities in technologies used for the LHeC and the specified experiments.

3.2. Geometry of The LHeC Detector

3.2.1. Magnet system

The LHeC magnet system design (Fernandez et al. 2012, Tommasini et al. 2012) presents a solenoid that can provide a magnetic field of 3.5 T. It is placed between electromagnetic calorimeter and hadronic calorimeter with a length of 5.7 m and a free bore of 1.8 m to house the tracker and EMC detectors. See Figure 3.1 and 3.9.

In the Linac-Ring option an additional 0.3 T, provided by the two dipoles, is also required to bend the e-beam into the IP. As can be seen in Figure 3.1, each of the dipoles is divided into two sections: the superconducting inner part (with the same bore as the solenoid) and the outer section magnet with a bore of 0.3 m stands on the beamline either side of the detector. The inner superconducting dipoles and solenoid, by the support of a common Al cylinder, are integrated into one cryostat (Figure 3.2) equipped with thermal shields.

Al stabilized NbTi/Cu Rutherford cable is used in the inner superconductor dipoles (Russen-schuck et al. 2012), whereas the outer dipoles are normal-conducting iron based. A 14 mm sized tube is attached to the outer surface of the support cylinder which is used for forced liquid helium to cool the solenoid and dipoles. Moreover, a 0.3 mm thick double layer of polyimide/glass tape is used for conductor insulation. In the FLUKA simulations, in addition to the definition of mentioned materials, the 3.5 T is switched on for the regions under the magnet system.

The technology used for the LHeC solenoid has been proven well by the experiments like ATLAS (Yamamoto et al. 2008) and CMS (Acquistapace et al. 1997). Some of the dimensions and characteristics of this section listed in Table 3.1.

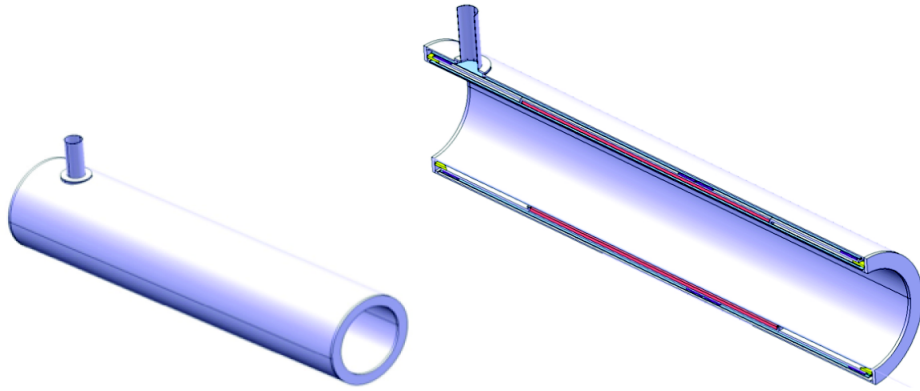


Figure 3.2. Te cryostat of the LHeC magnet system.

Table 3.1. Dimensions of the LHeC magnet system.

Parameter	Value	Unit
Cryostat inner radius	0.90	<i>m</i>
Length	10.0	<i>m</i>
Outer radius	1.140	<i>m</i>
Coil windings inner radius	0.960	<i>m</i>
Length	5.70	<i>m</i>
Thickness	60.0	<i>mm</i>
Support cylinder thickness	0.030	<i>mm</i>
Conductor sect., Al-stabilized NbTi/Cu insulation	30.0×6.8	<i>mm</i> ²
Length	10.8	<i>km</i>
Superconducting cable sect., 20 strands	12.4×2.4	<i>mm</i> ²
Superconducting strand ϕ Cu/NbTi ratio = 1.25	1.24	<i>mm</i>

3.2.2. Tracking detector

The tracking detectors which are the most inner part of the LHeC detector baseline layout, are all silicon devices with very high resolution. Covering the pseudorapidity of $-4.8 < \mu < 5.5$, the tracker is located inside the electromagnetic calorimeter and under a solenoidal field of 3.5 T (Fernandez et al. 2012). Figure 3.3 shows the baseline layout of the tracking detector which includes the sub-parts of Central Pixel Tracker (CPT), Central Silicon Tracker (CST), Central Forward/Backward Tracker (CFT, CBT) and Forward/Backward Silicon Tracker (FST, BST). The tracker is kept as small as possible in

radius for the requirements of the tracking detector and also the limitation given by the magnet system.

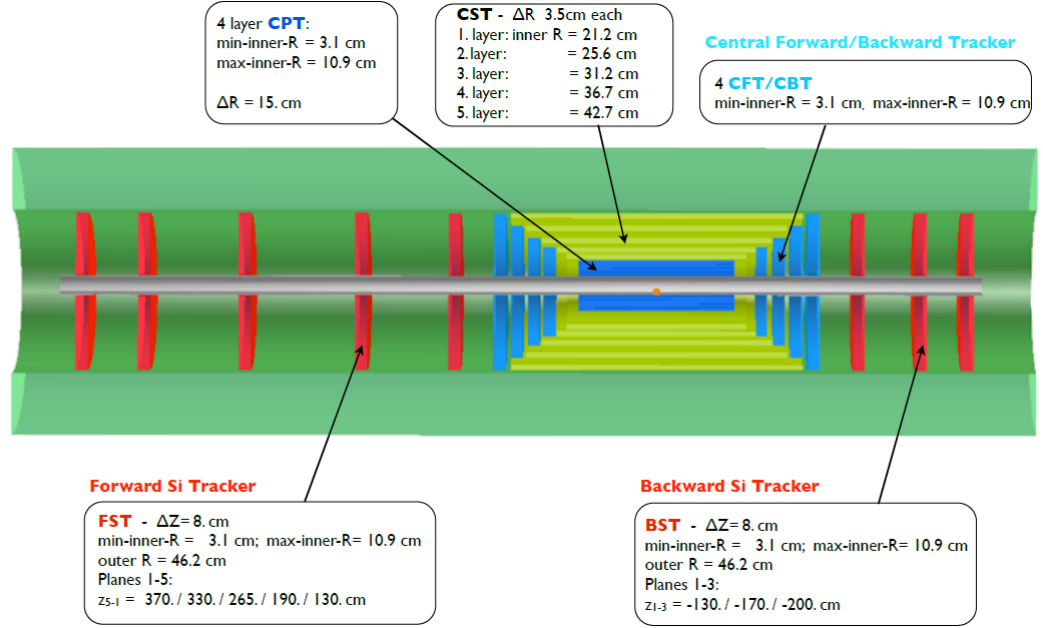


Figure 3.3. The $r - z$ view of Tracker detectors and Electromagnetic-Calorimeter for the LHeC baseline layout.

3.2.2.1. Pixel detector

The main task of the pixel detector is the reformation of secondary vertices and generation of track seeds for the reformation in the full tracker. The LHeC tracker detector uses a pixel detector with a resolution of $\sigma_{pix} \approx 8 \mu m$ in position. The barrel part includes four Si-Pixel layers (CPT1-CPT4) with minimum radii of 3.1, 5.6, 8.1 and 10.6 cm, which are placed as close to the beam pipe as possible. The ΔR is 2 cm for each layer (Fernandez et al. 2012).

Figure 3.4 illustrates the module used in the ATLAS pixel detector (Aad et al. 2008) which is assembled of sensor tile, front-end electronics chips (FE), flex-hybrid, module control chip (MCC) and a flexible foil called pigtail (Alam et al. 1998). The geometry used for the CPT simulation is given in Table 3.2, while the material composition is based on the pixel detector used in the ATLAS detector.

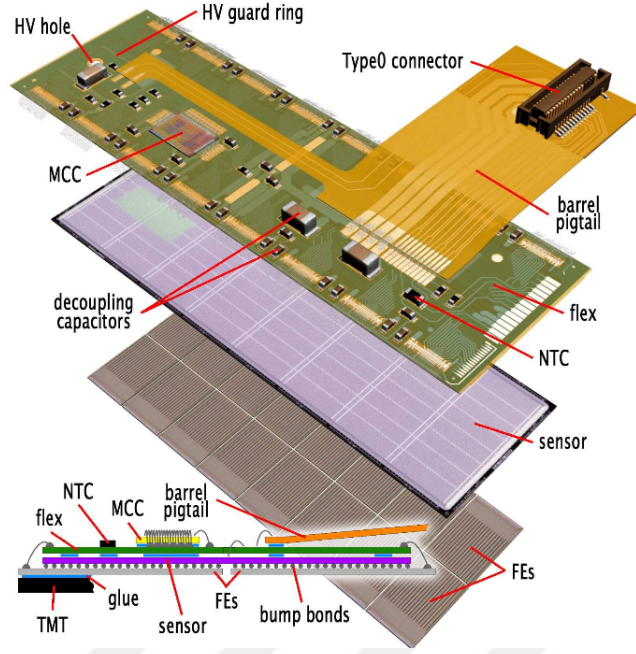


Figure 3.4. The exploded view of a barrel pixel for ATLAS detector full module (Alam et al. 1998).

Table 3.2. Summary of the Central Pixel and Central Strip Tracker (CPT/CST).

Cen. Barrel	CPT1	CPT2	CPT3	CPT4	CST1	CST2	CST3	CST4	CST5	
Min. R [cm]	3.1	5.6	8.1	10.6	21.2	25.6	31.2	36.7	42.7	
Min. θ [°]	3.6	6.4	9.2	12.0	20.0	21.8	22.8	22.4	24.4	
Max. $ \eta $	3.5	2.9	2.5	2.2	1.6	1.4	1.2	1.0	0.8	
ΔR [cm]	2	2	2	2	3.5	3.5	3.5	3.5	3.5	
$\pm z$ -length [cm]	50	50	50	50	58	64	74	84	94	
Project [m^2]	1.4								8.1	

3.2.2.2. Strip detector

Si-Strixel detectors, as depicted in Figure 3.3, include 5 central barrel layers (CST1-CST5) with a resolution of $\sigma_{strixel} \approx 12\mu m$. Minimum radii of the layers are 21.2, 25.6, 31.2, 36.7 and 42.7 cm. The LHeC Strip detectors use silicon module (Figure 3.5), which is currently functional in the CMS tracker (Borrello et al. 2003, Azzurri 2006). A layout of the silicon strip (2-in-1 design) is shown in Figure 3.6. The simulation of this region is based on the information given in Table 3.2 along with materials used in the silicon strip module.

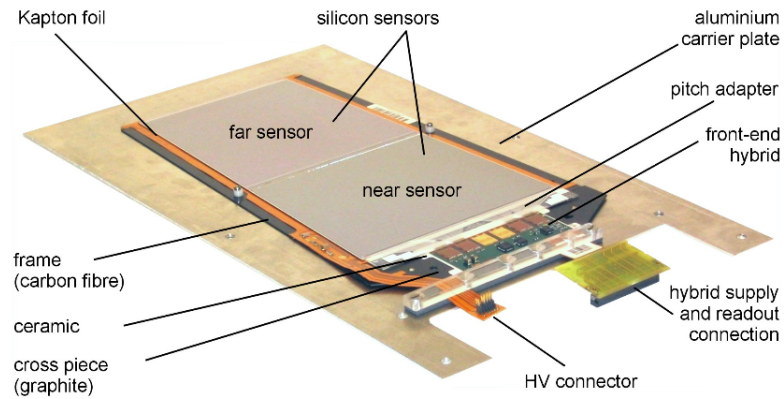


Figure 3.5. A layout of a silicon strip used in the CMS Tracker (Kaußen 2008).

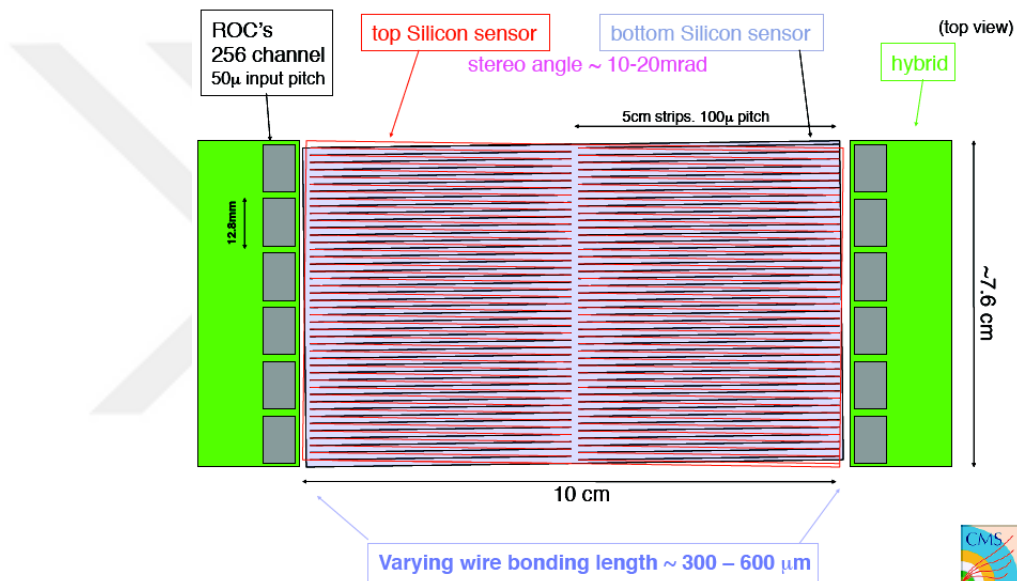


Figure 3.6. A layout of the 2-in-1 strip sensor design used in the CMS tracker module.

3.2.2.3. The endcaps

The central tracker is finally completed by four disks of endcaps in both Central Forward and Central Backward Trackers (CFT-CBT). The dimensions of each disk are summarized in Table 3.3.

Furthermore, five wheels of Forward Silicon Tracker (FST) and three wheels of Backward Silicon Tracker (BST) are positioned in the forward and backward directions of the tracker respectively (Figure 3.3). Tabel 3.4 gives more information about these wheels.

Table 3.3. Summary of the Central Forward and Backward Trackers (CFT/CBT).

Cen. Barrel	CFT1	CFT2	CFT3	CFT4	CBT1	CBT2	CBT3	CBT4
Min. R [cm]	3.1	3.1	3.1	3.1	3.1	3.1	3.1	3.1
Min. θ [°]	1.8	2.0	2.2	2.6	177.4	177.4	178	178.2
at z [cm]	101	90	80	70	-70	-80	-90	-101
Max./Min. η	4.2	4.0	3.9	3.8	-3.8	-3.9	-4.0	-4.2
Δz [cm]	7	7	7	7	7	7	7	7
Project [m^2]		1.8				1.8		

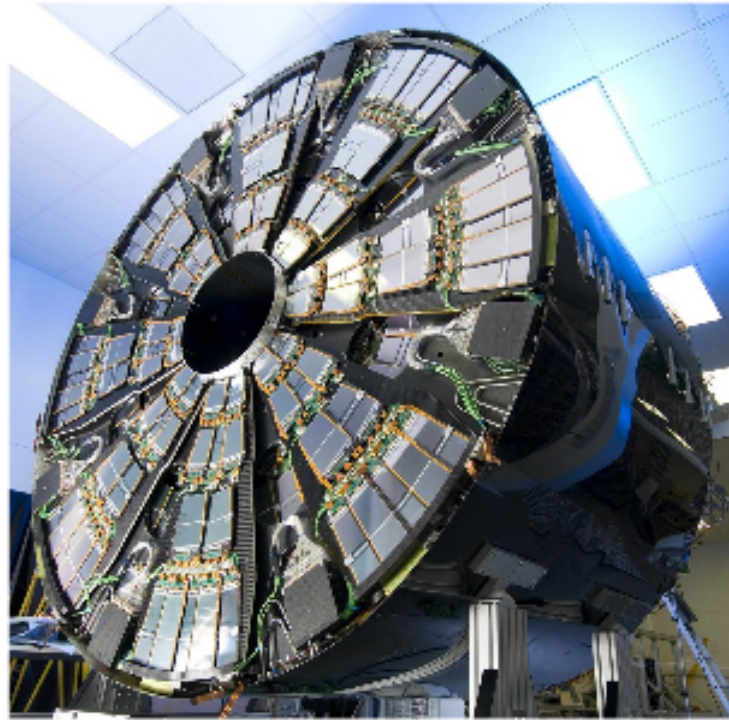


Figure 3.7. A fully assembled end-cap of CMS (Widl 2008).

The BST uses Si-Strip, while in the five wheels of FST, Si-Pixel or Si-Strixel detectors may have to be used (Fernandez et al. 2012). In this work, for both FST and BST, Si-Strip detectors are simulated. The materials which are less in amount and does not have a significant radiation length were neglected in the simulation. Figure 3.5 demonstrates a template of the Si-Strip module used in the CMS. A fully assembled end-cap of the CMS detector is depicted in Figure 3.7.

Table 3.4. Summary of the Forward and Backward Silicon Trackers (FST/BST).

Cen. Barrel	FST5	FST4	FST3	FST2	FST1	BST1	BST2	BST3
Min. R [cm]	3.1	3.1	3.1	3.1	3.1	3.1	3.1	3.1
Min. θ [°]	0.48	0.54	0.68	0.95	1.4	178.6	178.9	179.1
at z [cm]	370	330	265	190	130	-130	-170	-200
Max./Min. η	5.5	5.4	5.2	4.8	4.5	-4.5	-4.7	-4.8
Outer R [cm]	46.2	46.2	46.2	46.2	46.2	46.2	46.2	46.2
Δz [cm]	8	8	8	8	8	8	8	8
Project [m^2]		3.3					2.0	

3.2.2.4. Powering and cooling

The LHeC powering and cooling system, as pointed in LHeC CDR, can use the current LHC installations (Fernandez et al. 2012). For instance, ALICE and CMS pixel detectors have adopted so far C_6F_{14} monophasic liquid cooling-systems as the baseline. Although fluorocarbon fluid has the features of excellent stability, good thermal properties and high electrical resistance, the CMS upgrade for the cooling system has used CO_2 to have a much more lightweight and effective cooling system (König 2009, Daguin et al. 2012). Figure 3.8 shows the mechanics layout for the CMS inner barrel tracker upgrade form, which CO_2 is used instead of fluorocarbon.

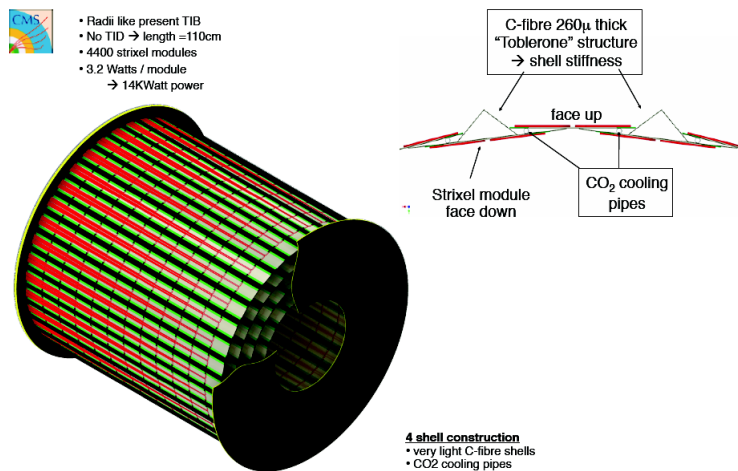


Figure 3.8. The mechanics layout designed for the CMS inner tracker.

3.2.3. Calorimetry

The LHeC calorimetry, illustrated in Figure 3.9, is located behind the tracker detectors and has two parts of electromagnetic and hadronic calorimeters covering rapidity region up to $|\eta| < 5.5$. The Electromagnetic Calorimetry (EMC) is based on liquid argon technology, while Hadronic Calorimetry (HAC) uses scintillating tiles technology. Taking into account the electromagnetic and hadronic showers, a high enough radiation length of $X_0 = 30$ and interaction length of $\lambda_I = 10$ are considered for the EMC and HAC respectively.

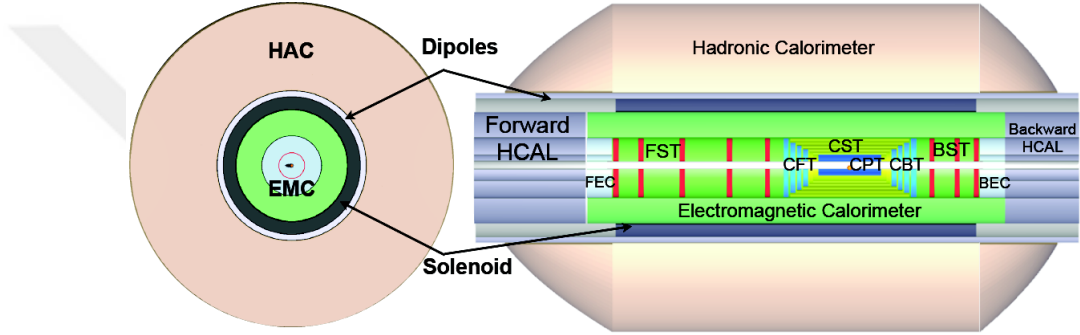


Figure 3.9. $x - y$ and $r - z$ view of the LHeC calorimetry, EMC (green) and HAC (pink).

3.2.3.1. Electromagnetic calorimeter

The electromagnetic calorimeter of the LHeC experiment is a Liquid Argon (LAr) sampling calorimeter with accordion shaped electrodes, subdivided into three parts: central Electromagnetic barrel (EMC) and Forward and Backward Electromagnetic Calorimeters (FEC/BEC), see Figure 3.9. It covers a rapidity range of $2.8 < \eta < -2.3$ and based on the electromagnetic calorimeter currently used by the ATLAS (Alam 2005, Wilkens 2009). LAr has been chosen because of its intrinsic linear behavior, the stability of the response over the time and radiation tolerance. A detail of the accordion-electrode structure of ATLAS EMC is presented in Figure 3.10.

As seen in Figure 3.10, a cell consists of a lead absorber plate, a copper/Kapton readout electrode and the liquid Argon in both sides (Buchanan et al. 2008, Fernandez et al.

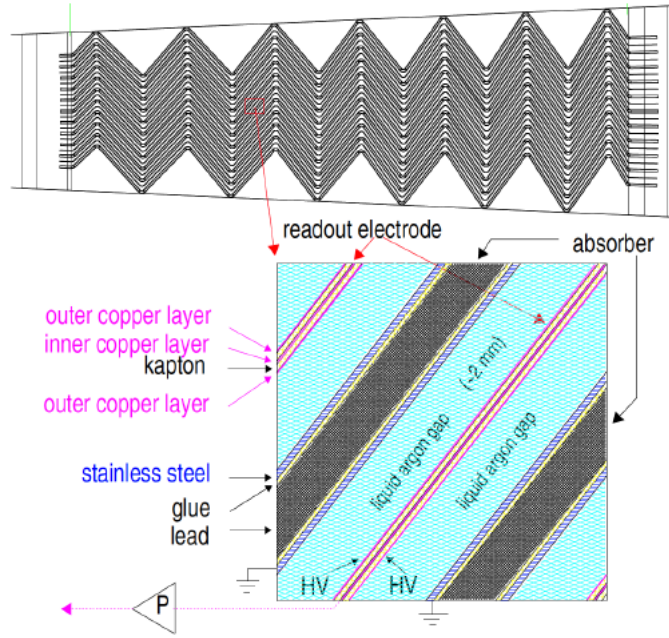


Figure 3.10. Accordion structure of ATLAS LAr Calorimeter with a longitudinal view of its one cell.

2012). Si-W modules ($X_0 = 30$) and Si-PB modules ($X_0 = 25$) are used in the FEC and BEC respectively.

Some preliminary simulations of the EMC have been already presented in CDR using GEANT4 (Agostinelli et al. 2003) and FLUKA. Using almost the same approach, this simulation defines a composite material based on the X/X_0 of all used materials like LAr, Cu, Lead, Stainless steel, Kapton, glue etc. A 3D view of the accordion structure of the ATLAS LAr Calorimeter is shown in Figure 3.11. Further details about EMC are summarized in Table 3.5.

Table 3.5. The details of the LHeC electromagnetic calorimeter.

E-Calo parts	FEC1	FEC2	EMC	BEC2	BEC1
Min. Inner radius R [cm]	3.1	21	48	21	3.1
Min. polar angle θ [°]	0.48	3.2	6.6/168.9	174.2	179.1
Max./Min. η	5.5	3.6	2.8/-2.3	-3	-4.8
Outer R [cm]	20	46	88	46	20
z-length [cm]	40	40	660	40	40
Volume [m^3]		0.3	11.3	0.3	

Table 3.6. Summary of the hadronic calorimeter barrel part dimensions.

H-Calo barrel part	FHC4	HAC	BHC4
Inner radius R [cm]	120	120	120
Outer radius R [cm]	260	260	260
z-length [cm]	217	580	157
Volume [m^3]		121.2	

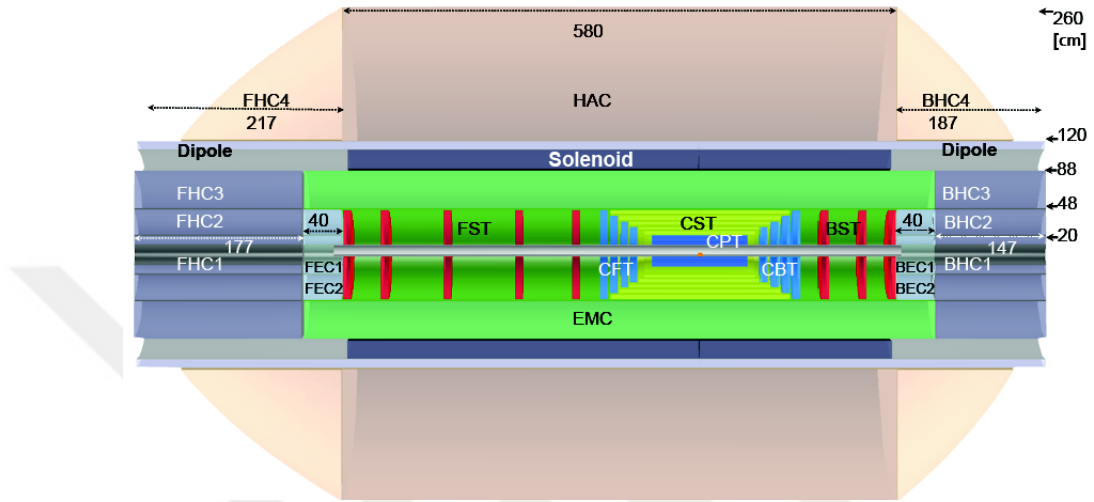


Figure 3.12. An $r - z$ view of HAC, FHC1-FHC3, BHC1-BHC3 of the LHeC detector.

The forward and backward parts of the calorimeter (FHC, BHC) are exposed to high level of radiation environment. Therefore, Tungsten with short radiation length is used as the absorber material. Copper can be used as an alternative in the BHC. Table 3.7 summarize the detail of the FHC and BHC.

Table 3.7. Summary of the FHC and BHC dimensions.

H-Calo parts Inserts	FHC1	FHC2	FHC3	BHC3	BHC2	BHC1
Min. Inner radius R [cm]	11	21	48	48	21	3.1
Min. polar angle θ [$^\circ$]	0.43	2.9	6.6	169	175.2	179.3
Max./Min. η	5.6	3.7	2.9	-2.4	-3.2	-5
Outer R [cm]	20	46	88	88	46	20
z-length [cm]	177	177	177	117	117	117
Volume [m^3]		4.2			2.8	

3.2.4. Muon Detectors

The muon layers are the outermost component of the LHeC detector. A 3D view of the LHeC detector surrounded by the three muon layers is demonstrated in Figure 3.13. Depending on the central detector, the LHeC muon detector has various options like muon tagging, combined muon momentum measurement and standalone momentum measurement which are yet to be finalized for the baseline layout. The first option, muon tagging, is based on the LR design of central detector using the residual magnetic field of the central solenoid. It considers three layers each include a double layer for triggering along with another layer for precision measurements, see Figure 3.14.

This method is commonly used in HEP experiments. In the ATLAS and CMS experiments; Drift Tubes (DT) and Cathode Strip Chambers (CSC) are used to obtain the measurement of position and momentum of the muons while Resistive Plate Chambers (RPC) are dedicated to triggering and second coordinate measurements (Fernandez et al. 2012).

In the CMS muon system, DTs are used in the central barrel region, CSCs in the endcap region and RPC is used in both the barrel and endcaps (S Chatrchyan 1997). For the simulation of muon layers, based on the traditional technology used by CMS and ATLAS, Al layers, Ar/CO_2 gas mixture, W-Re wire and other used materials detailed (Arai et al. 2008, Collaboration 2010), are considered for DTs. While in the case of endcaps, anode wires with copper strips (cathode) within the gas volume are included in the simulation. The gas mixtures ($C_2H_2F_4$), Bakelite electrodes and readout strip are simulated for the RPC (Thyssen 2012, Hadjiiska et al. 2013). Further studies on the detail of LHeC muon system design can help us to improve the accuracy of the simulations.

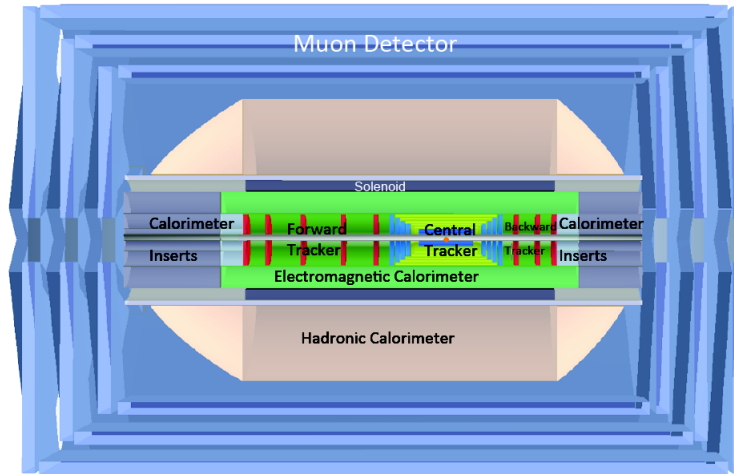


Figure 3.13. A full view of the baseline detector in the $r - z$ plane with all components shown. The dimensions are $\approx 14 \text{ m} \times 9 \text{ m}$.

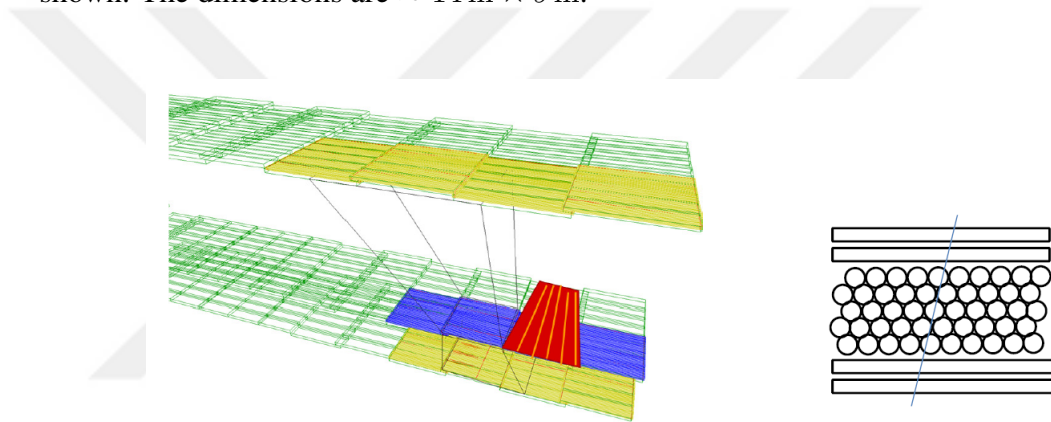


Figure 3.14. An artist 3D view of the projective arrangement of the barrel layer muon chambers (left). A schematic view of the cross section of one of the chambers (right) (Fernandez et al. 2012).

3.3. The FLUKA Monte Carlo Code

The FLUKA Monte Carlo Code is a well-known transport code widely used for calculation of particle transport and interactions with matter. The name of FLUKA code stands for FLUKtuierende Kaskade (Fluctuating Cascade) which was first written in 1962 by Johannes Ranft and later on, it was developed by a collaboration of CERN and INFN in 2003 (Rata et al. 2016).

FLUKA can transport particles over a wide energy range of 1 keV to thousands of TeV. It is capable of transporting about 60 different particles; neutrinos, muons with different

energies, hadrons with energy up to 20 TeV and all the corresponding antiparticles, neutrons down to thermal energy and heavy ions. It covers an extensive range of applications spanning from proton and electron accelerator shielding to target design, calorimetry, activation, dosimetry, detector design, cosmic rays, radiotherapy, etc. (T.Böhlen 2005). In this study, the geometry of the LHeC detector, as explained in section 3.2, was constructed in FLUKA. The new defined materials in the simulation are based on their X/X_0 in consideration of the required radiation length X_0 or interaction length λ_I for each sub-detector, as reported in LHeC CDR. For simulation of radiation environment, the required data was generated by PYTHIA 6 (Sjostrand et al. 2006) as a result of 7 TeV proton and 120 GeV electron beam collisions. The pseudorapidity η and momentum of particles in the generated data is drawn in ROOT Data analysis program (Figure 3.16) (Brun and Rademakers 1997).

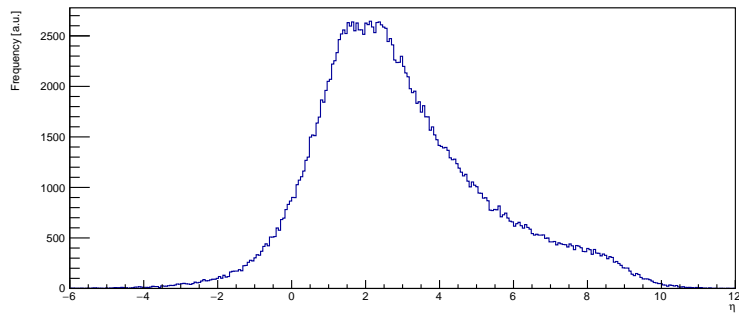


Figure 3.15. The pseudorapidity of particles in ep data generated by PYTHIA 6.

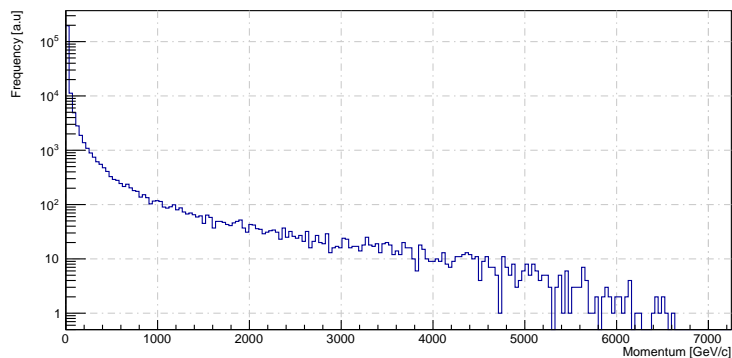


Figure 3.16. The momentum of particles in ep data generated by PYTHIA 6.

4. SIMULATION RESULTS

4.1. Radiation Environment at the LHeC Detector

FLUKA predictions for significant radiation estimators are discussed in this chapter. Section 4.1.1 presents the fluence of some particles which are more effective in radiation damage studies. The fluence of energy and ionizing dose are given in section 4.1.2. Finally, section 4.12 is dedicated to Non-Ionizing Energy Loss (NIEL) which let us study the displacement damage in semiconductors or other electronic devices. The simulation results in this study are performed per primary weight (unit primary particle statistical weight) (T.Böhlen 2005). A detailed presentation of cross section studies at the LHeC is helpful for the normalization and improvement of the results.

4.1.1. Particle Fluence

Fluence is one of the main monitoring parameters in radiation background studies. It is defined as the number of particles or amount of energy passing through a surface per unit area (Daquino et al. 2006). Another definition is the track length per unit volume, which in both cases has a unit of m^{-2} . In the matter of energy, it is called fluence of energy with a unit of $J.m^{-2}$. There are radiations created from different particles in the detector, however, some of them like neutrons, protons, hadron with energy greater than 20 MeV, 1 MeV neutron equivalent etc. have more influence on damage effects and are of high importance in radiation background studies. Investigating the charged particles is useful for studying detector occupancy. Figure 4.1 demonstrates the fluence of all charged particles per primary weight at the LHeC detector. As it is obvious from the figure, the charged particles constituted during the collision of electron and proton beams, have a higher radiation in the inner detector especially in the forward region due to higher energy of the proton beam.

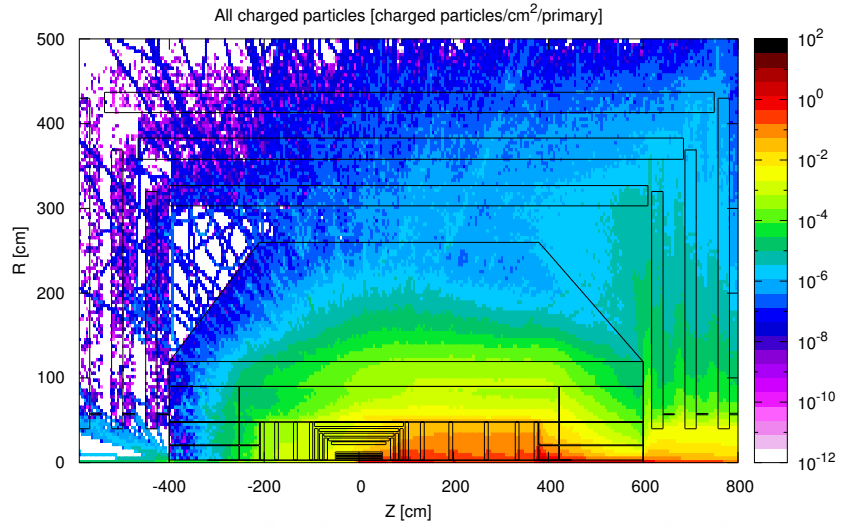


Figure 4.1. The fluence of all charged particles [$\text{particles}/\text{cm}^2/\text{sec}$] in the LHeC detector.

Shown in Figure 4.2 is the fluence of hadrons with energy greater than 20 MeV. Due to the high energy of proton beam (7 TeV), the formation of energetic hadrons are expected in the forward regions of the detector, especially in the inner detector. Background simulation for hadrons with energy greater than 20 MeV is important for studying the single event upsets.

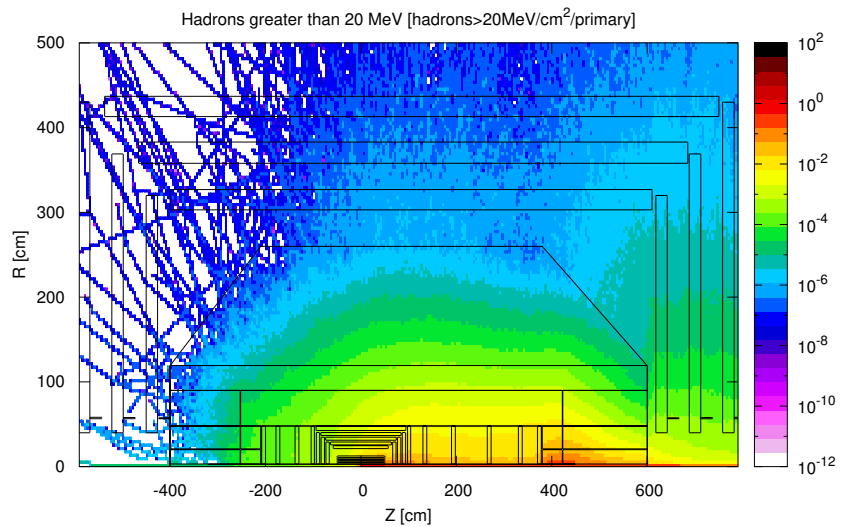


Figure 4.2. The distribution of hadrons with energy greater than 20 MeV.

The contour map presented in Figure 4.3 is neutron fluence in the LHeC detector. A higher flux of neutrons is observed in the inner detector, particularly in the FEC and FHC regions which utilize the radiation-hard W-Si and Cu-Si modules. Among the neutral hadrons, neutrons which are largely formed in nuclear evaporation, have a considerably longer lifetime and it is only nuclear scattering which is effective in their attenuation allowing them to travel large distances. Therefore, in High Energy Physics, detector damages due to neutron background is a well-known issue since few regions of the detector are save from the radiations (Huhtinen and Aarnio 1995, Arratia Munoz 2016), as it is also the case for the LHeC detector. To reduce the radiation damages, neutron shielding materials like stainless steel are largely used in the HEP experiments (Linnik et al. 2017).

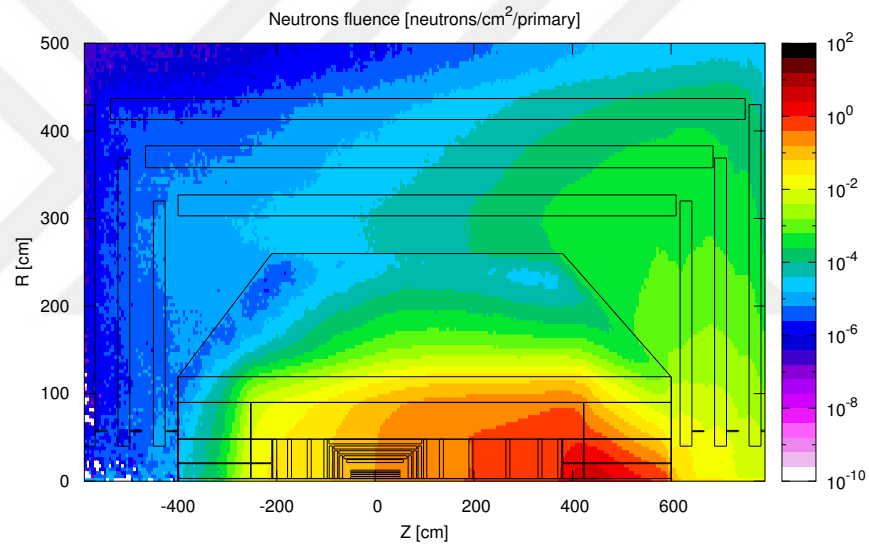


Figure 4.3. The neutrons fluence in the LHeC detector.

Given in Figure 4.4 is the proton fluence which is quite different as that of neutrons. Protons predominantly lose their energy in the hadronic calorimeter. However, the hadronic cascade created by the high energy proton beams causes more intense proton fluence in the forward calorimeters (FEC and FHC). Figure 4.5 presents the photon fluence showing a higher radiation in the FST and FEC regions. Photons, which are investigated in the EMC, have many formation sources like electromagnetic cascade and neutron capture reactions (von Holtey 1992, Huhtinen and Aarnio 1995). The neutron capture can also be seen from the similarity in the photon and neutron fluences. See Figure 4.5 and 4.3.

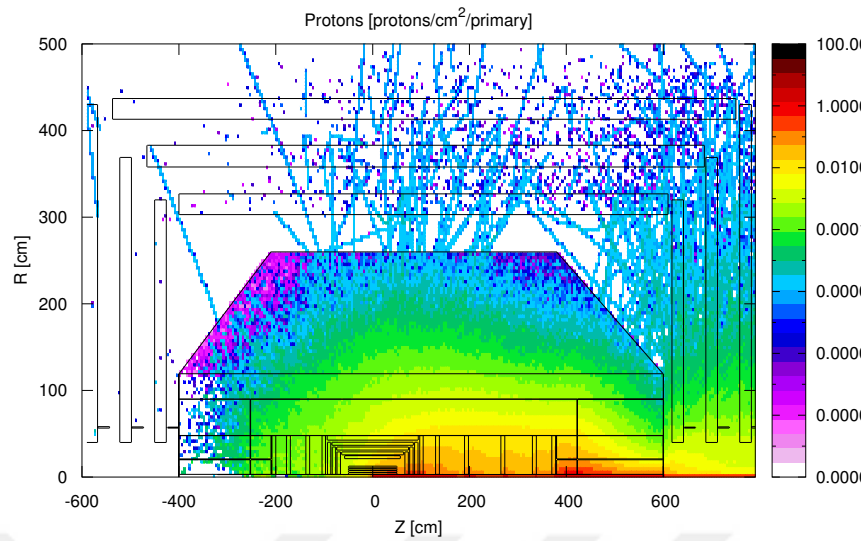


Figure 4.4. The protons fluence in the LHeC detector.

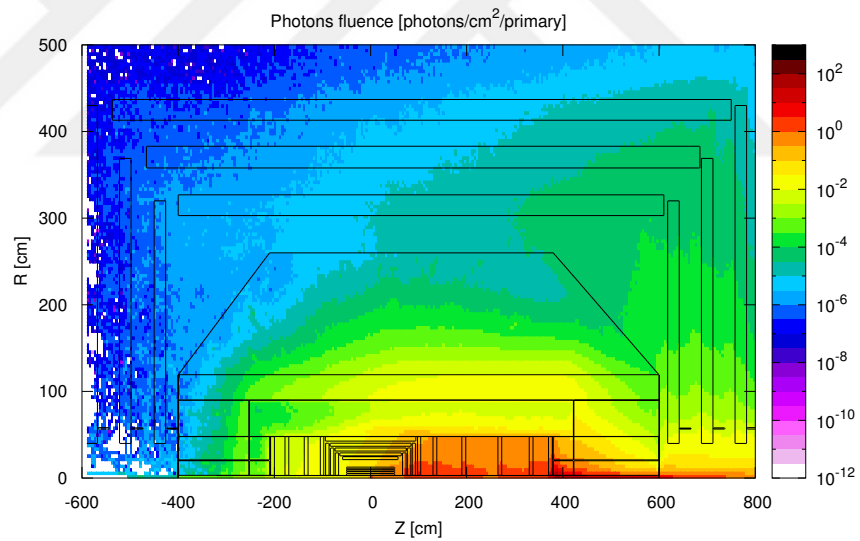


Figure 4.5. The photons fluence in the LHeC detector.

Figure 4.6 shows the distribution of all pions. Compared to the other particle fluences, muons have a quite different contour fluence. See Figure 4.7. Their trajectories are rather straight reaching the muon detector. However, similar to other heavy particles, muons have an intense background in the forward regions of the detector.

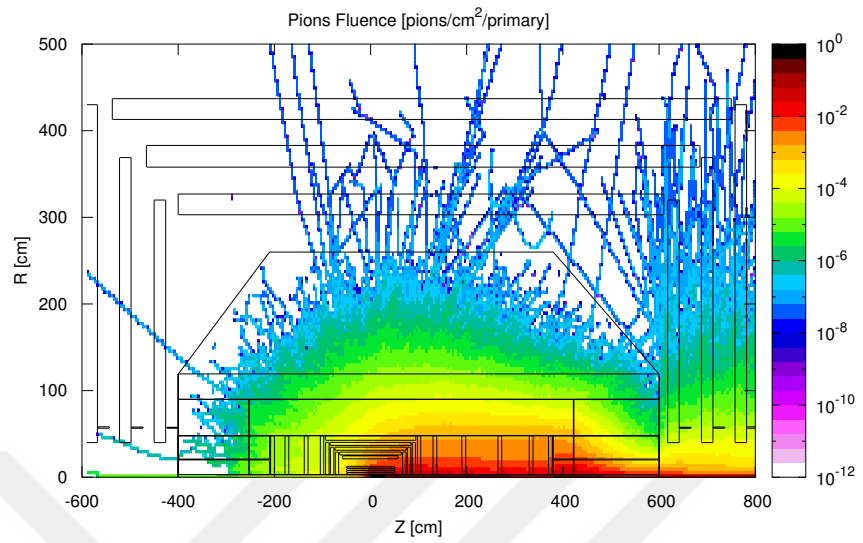


Figure 4.6. The pions fluence in the LHeC detector.

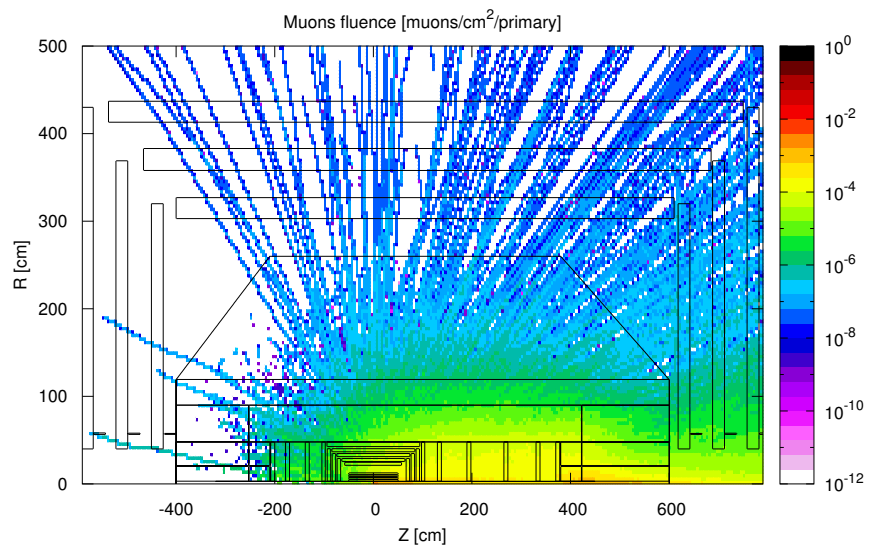


Figure 4.7. The muons fluence in the LHeC detector.

4.1.2. Energy Distribution and Ionizing Dose

Figure 4.8 shows the contour map of deposited energy in the different regions of the LHeC detector. A significant energy deposition is seen in the inner detector and calorimeters. This contour is the result of ENERGY scoring in FLUKA USRBIN, which in the case of energy fluence, specifies the Kinetic energy (Ferrari et al. 2005).

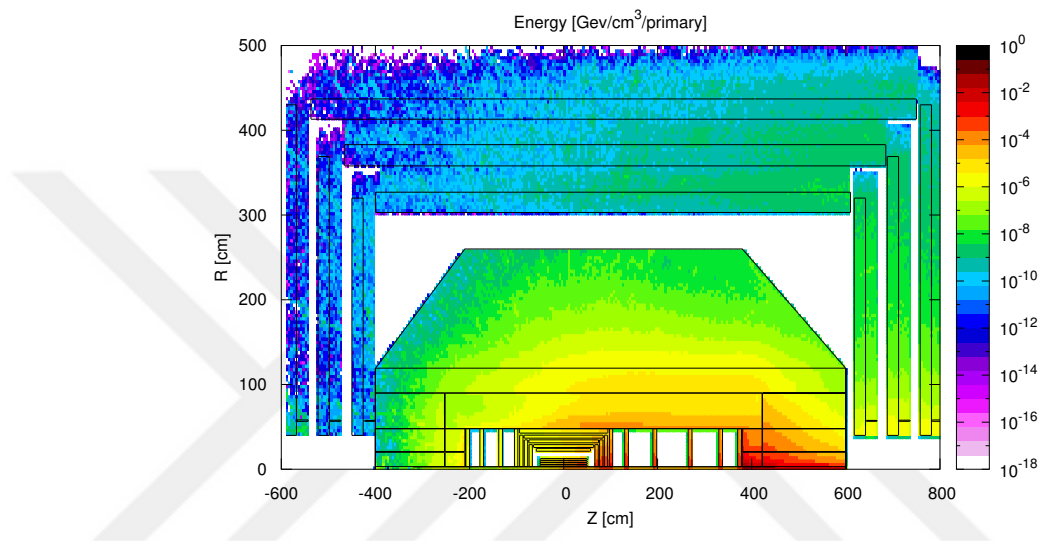


Figure 4.8. Energy distribution in the LHeC detector.

In radiation damage studies, particularly in surface damages calculations, ionizing radiation dose defined as the energy delivered in a volume per unit of the volume mass, is of central importance. The unit becomes Joule/Kg/Sec which is commonly given in Gray/year (Gy/Yr). Gray is the unit of absorbed dose and 1 Gy = 1 Joule/Kg (Huhtinen 1996, Baranov et al. 2005). All energy loss mechanisms are included in Dose. However, ionization is the most common mechanism which silicon and other electronic devices are subject to its defects especially in the surface layer. For displacement damage, non-ionizing energy loss as explained in the next section is considered. Figure 4.9 demonstrates the dose distribution in the LHeC detector in GeV/gr/primary, the unit considered by FLUKA. As seen in the figure, tracker system is exposed to a more intense ionizing radiation which causes surface damage effects.

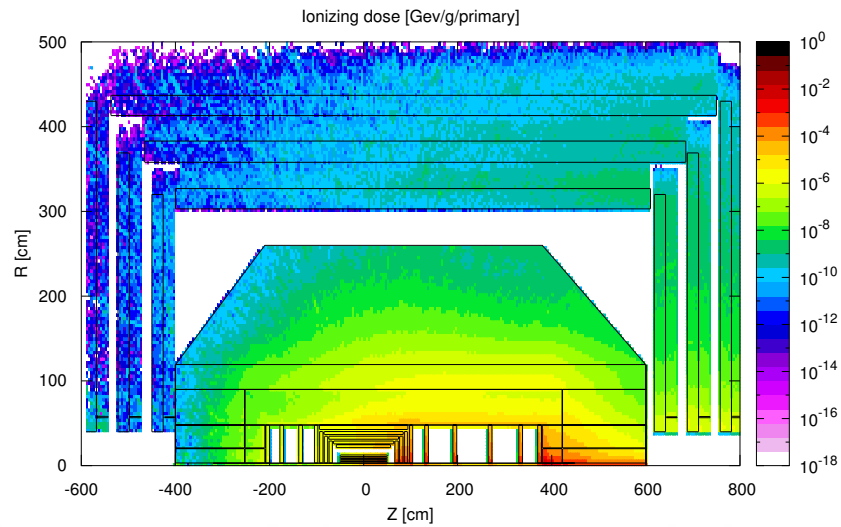


Figure 4.9. Dose distribution in the LHeC detector.

4.1.3. Displacement Damage and NIEL

The LHeC detector widely uses silicon especially in the tracker system like silicon pixel and silicon strip. Therefore, their degradation due to displacement damage is of huge importance for the LHeC radiation environment. Generated radiations in the detector damage the semiconductors and electronics either by ionizing energy loss in the surface level, as explained in the previous section, or by the displacement damage known as bulk damage. Bulk damage is introduced as a deformity of the crystal lattice of a semiconductor which leads to some changes in the characteristics of the device (Huhtinen 1996, Mallows et al. 2016).

Studies have shown that damage effect is roughly proportional to the displacement damage cross section (MeVmb) which is equivalent to the Non-Ionizing Energy Loss-NIEL ($keV cm^2/gr$). This observation is also called "NIEL-scaling hypothesis". The Displacement damage cross section for 1 MeV neutrons flux is 95 MeVmb which has been set as a normalizing value by American Society of Testing and Materials (ASTM). Figure 4.10 shows the silicon damage function for some particles considering the normalizing value of $D_n(1MeV)=95$ MeVmb (Williams et al. 1994, Lindström 2003).

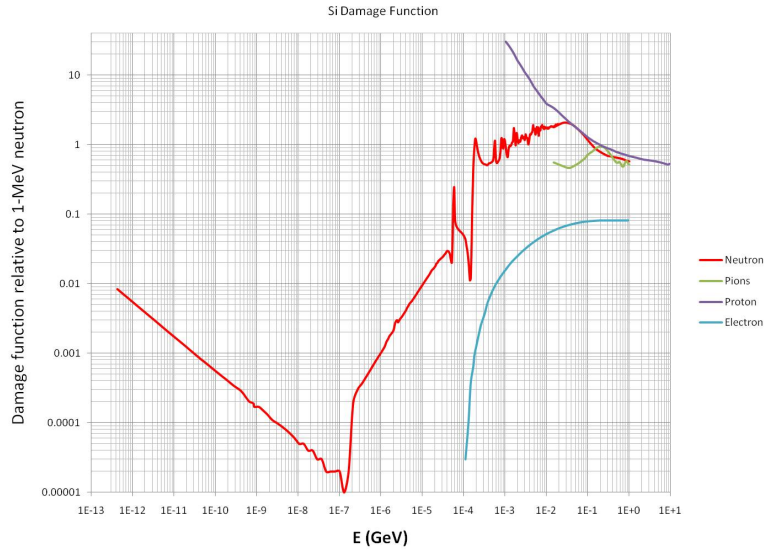


Figure 4.10. Displacement damage in Silicon for neutrons, pions, protons and electrons.

The equivalent 1 MeV neutron fluence prediction for the LHeC detector is given in Figure 4.11. In the LHeC inner tracker system, the most extreme damage fluences appear in the forward silicon tracker. The result of "NIEL-DEP" scoring in FLUKA for NIEL deposition in the LHeC detector is illustrated in Figure 4.12 describing "the energy loss due to atomic displacement (recoil nucleus) as a particle traverses a material" (T.Böhlen 2005).

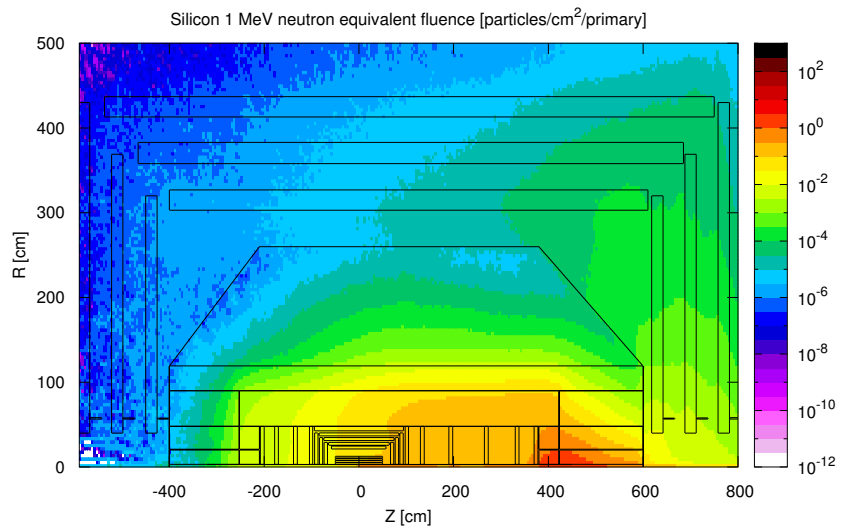


Figure 4.11. 1 MeV neutron equivalent fluence in the LHeC detector.

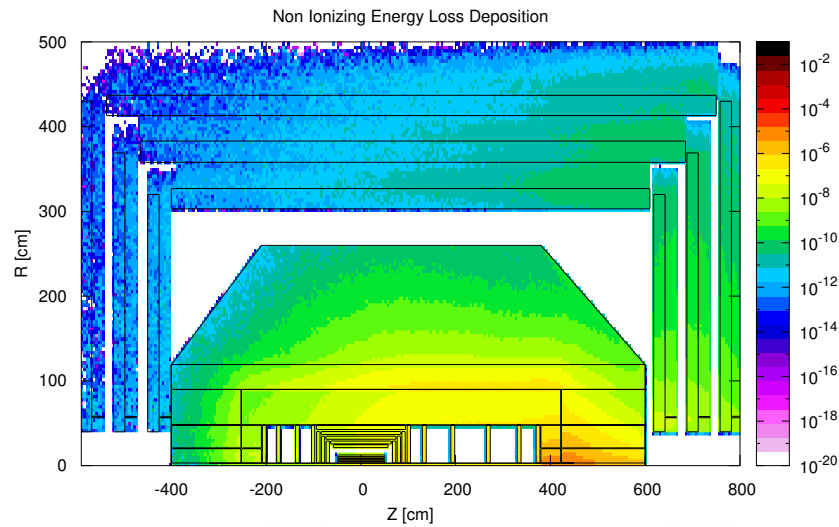


Figure 4.12. FLUKA prediction for the non-ionizing energy loss (GeV), in the LHeC detector.

4.2. Detector Response

For the simulation of detector response, 4×10^3 events of protons with 7 TeV energy were sent isotropically from IP of the detector. Afterwards, particles like neutrons, muons, hadrons greater than 20 MeV and all transportable particles in FLUKA, were tracked and presented. Moreover, the distributions of energy and 1 MeV neutron equivalent fluence were represented.

4.2.1. Particle Fluence

The interaction of protons with materials of the detector materials resulted in forming new particles which were then monitored by FLUKA. Given in Figure 4.13 is the fluence of all transportable particles in FLUKA. Since the events were sent isotropically, the contour fluence of particles is also equally distributed in the detector from the IP, as expected. The particles behave differently in the case of electron-proton data which is discussed in chapter 4. See Figure 4.1.

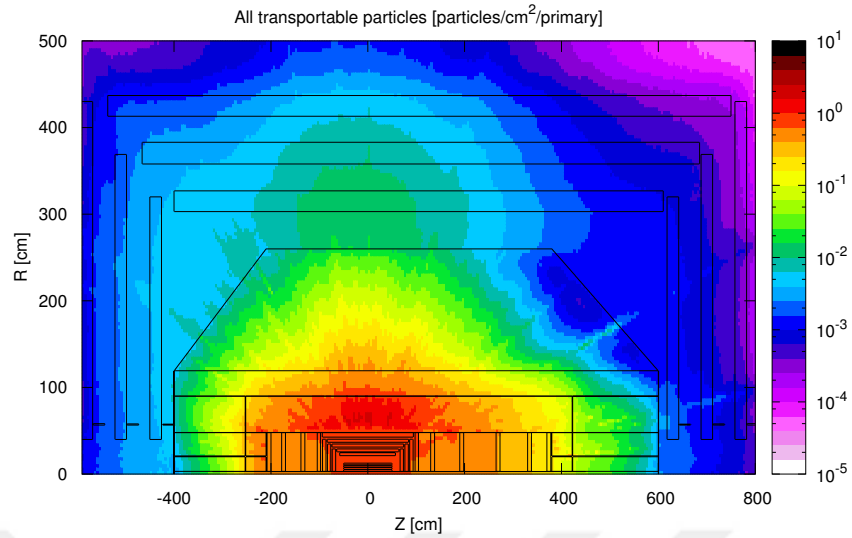


Figure 4.13. The distribution of all particles [particles/cm²/sec] in the LHeC detector as a result of 7 TeV proton events.

Figure 4.14 demonstrates the fluence of neutrons in the LHeC detector. As can be seen in the figure, the most serious background has been constituted in the innermost layers of the detector. Although, the fluence gradually becomes less intense in the distant regions.

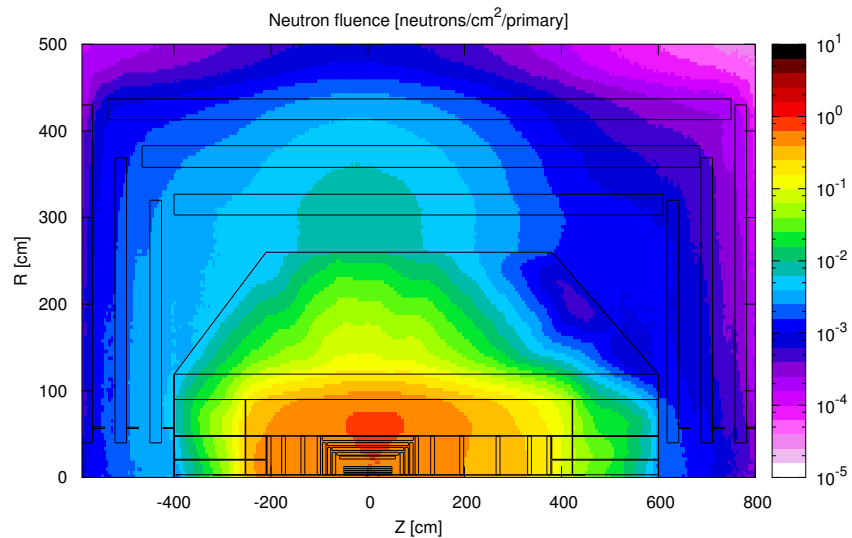


Figure 4.14. The neutrons fluence in the LHeC detector as a result of 7 TeV proton events.

The muons fluence is illustrated in Figure 4.15. By comparing the results with those from the ep data, one can simply observe the difference between contours which, regarding ep data, shows a higher background in the forward regions like FEC and FHC. While in the case of isotropic proton events, a radially-distributed fluence can be seen.

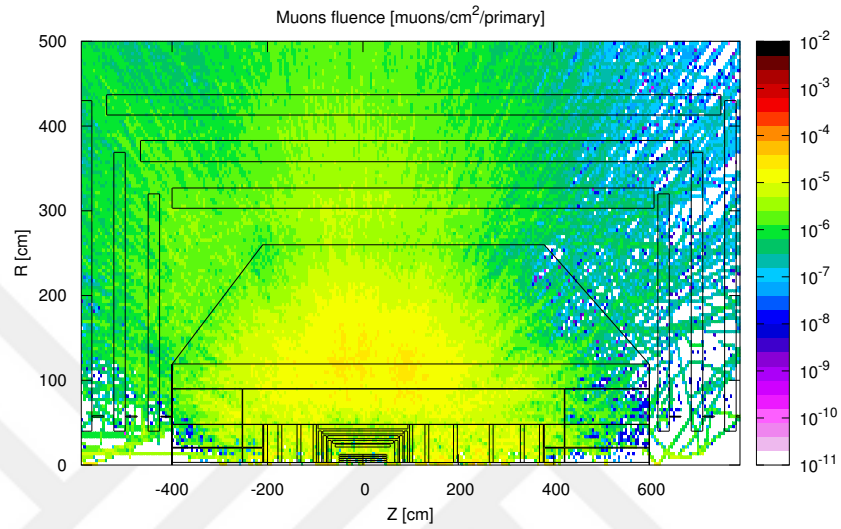


Figure 4.15. The fluence of muons at the LHeC detector as a result of 7 TeV proton events.

Finally, the fluence of hadrons with energy higher than 20 MeV is performed in Figure 4.16. More hadrons are constituted in the calorimetry which is due to hadronic showers formed by isotropic proton events sent from the IP. This varies in the matter of ep data, which similar to the other particles fluences, the harsh background is predicted in the forward calorimeters (Figure 4.2).

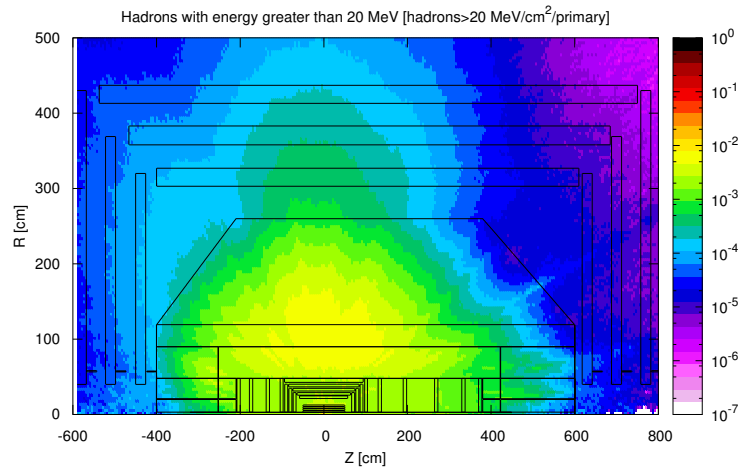


Figure 4.16. The distribution of hadrons with energy greater than 20 MeV [$\text{hadrons} > 20 \text{ MeV}/\text{cm}^2/\text{sec}$] in the LHeC detector as a result of 7 TeV proton events.

4.2.2. Energy Distribution

The energy fluence is shown in Figure 4.17. During the interaction of high energy protons with the detector materials, the energy deposition is seen in every region of the detector, especially in the EMC and HAC. More energy deposition is expected in the forward detectors during ep collision due to the high energy proton beams (Figure 4.8).

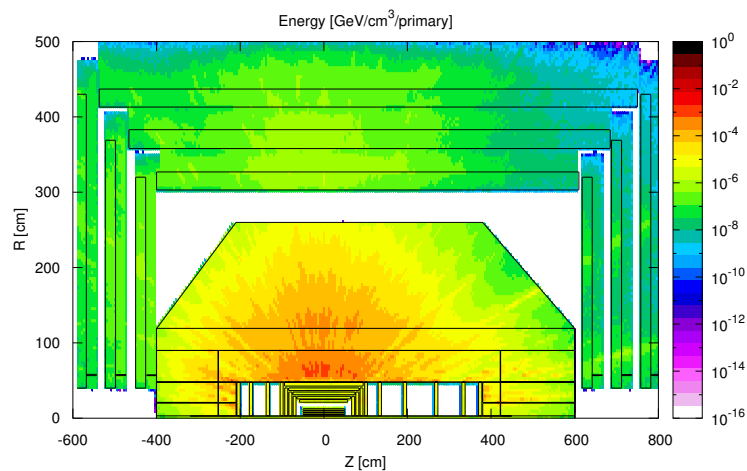


Figure 4.17. The distribution of energy [$\text{GeV}/\text{cm}^3/\text{sec}$] in the LHeC detector as a result of 7 TeV proton events.

4.2.3. 1 MeV Neutron Equivalent Fluence

Figure 4.18 presents the 1 MeV neutron equivalent fluence. The most affected part is the tracker system and EMC. As discussed in section 4.12, the higher radiations move to the forward regions, while the ep data is run.

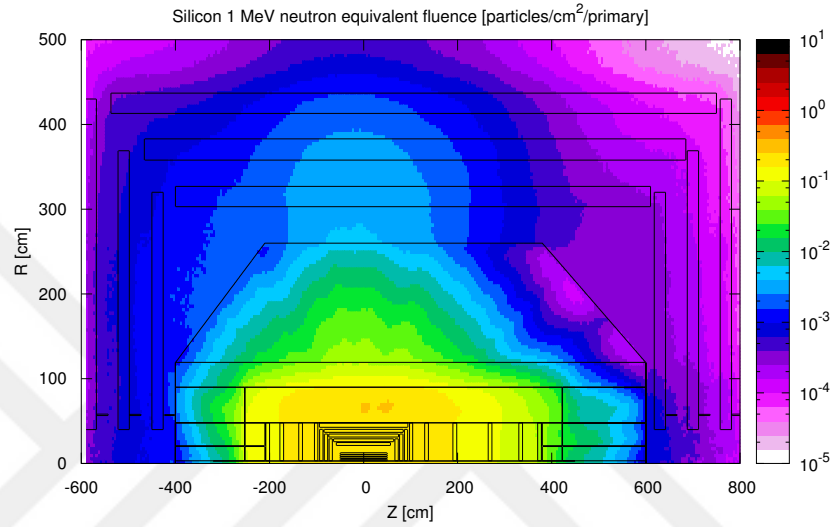


Figure 4.18. 1 MeV neutron equivalent flux in the LHeC detector as a result of 7 TeV proton events.

5. CONCLUSION

The LHeC with its extensive physics program is designed to collide the 7 TeV LHC proton/ion beam with a 60-140 GeV electron/positron beam accelerated in an ERL. The hermetic multi-purpose LHeC detector is subject to the radiations created due to the high luminosity and energy, mainly those regions which use semiconductor technology like tracker system.

In this work, the geometry of the LHeC detector, as detailed in LHeC CDR, was constructed in FLUKA. The new composite materials were then defined in consideration to the required radiation length and hadronic interaction length for each sub-detector. To present a preliminary simulation for the created radiations in the detector, an *ep*-data generated by PYTHIA6 was run in the virtual geometry.

The FLUKA predictions for the radiation estimators like particle fluence, Dose and NIEL, were performed showing a comparatively high radiation in the inner detector, especially in the FEC and FHC regions. These regions are exposed to the high energy proton beams coming from the backward detector. The FEC uses W-si modules which make it more resistant to the radiation effects. According to the simulations, a higher fluence of particles (protons, neutrons, muons, photons, etc.) is predicted in the tracker system and calorimeter, particularly in the forward regions of FST, FEC, and FHC. Likewise, in the event of energy, the inner detector and forward calorimeters (FEC and FHC) are predicted to expose more ionizing energy dose (Figure 4.9) which results in creating surface damages in the detector. This is also the case for non-ionizing energy loss NIEL resulting in bulk damage. The results are close to the simulations done in the CDR as in contour map of 1MeV neutron equivalent fluence.

Radiation background simulations are sensitive to the materials defined for each subsystem. In this work, some required information associated with the composition of materials (e.g. in silicon strips, muon chambers) were taken from CMS or ATLAS detectors based on some similarities in the technologies of both machines. The precision of the results can be improved when choices for the technology and designs of all sub-detectors are finalized.

REFERENCES

- Aad, G., Ackers, M., Alberti, F. A., Aleppo, M., Alimonti, G., Alonso, J., Anderssen, E. C., Andreani, A., Andreatza, A., Arguin, J.-F., Arms, K. E., Barberis, D., Barbero, M. B., Bazalova, M., Beccherle, R. B., Becks, K. H., Behera, P. K., Bellina, F., Beringer, J., Bernardet, K., Biesiada, J. B., Blanquart, L., Boek, J., Boyd, G. R., Breugnon, P., Buchholz, P., Butler, B., Caccia, M., Capsoni, A. C., Caso, C., Cauz, D., Cepeda, M., Cereseto, R., Cervetto, M., Chu, M. L., Citterio, M., Clemens, J. C., Coadou, Y. C., Cobal, M., Coccaro, A., Coelli, S., Correard, S., Cristinziani, M., Cuneo, S., D'Auria, S., Dameri, M., Darbo, G., Dardin, S., Lotto, B. D., Sanctis, U. D., Regie, J. B. D. V. D., Papa, C. D., Delpierre, P., Girolamo, B. D., Dietsche, W., Djama, F., Dobos, D., Donega, M., Dopke, J., Einsweiler, K., Eyring, A., Fasching, D., Feligioni, L., Ferguson, D., Fernando, W., Fischer, P., Fisher, M. J., Flick, T., Gagliardi, G., Galyaev, E., Gan, K. K., Garcia-Sciveres, M., Garelli, N., Gariano, G. G., Gaycken, G. G., Gemme, C., Gerlach, P., Gilchriese, M., Giordani, M. P., Giugni, D., Glitza, K. W., Gössling, C., Golling, T., Goozen, F., Gorelov, I., Gorfine, G., Grah, C., Gray, H. M., Gregor, I. M., Grosse-Knetter, J., Grybel, K., Gutierrez, P., Hallewell, G. D., Hartman, N., Havranek, M. 2008. ATLAS pixel detector electronics and sensors. *Journal of Instrumentation*, 3(07): P07007.
- Acquistapace, G., Andre, J., Bovard, A., Calvo, A., Campi, D., Cure, B., Delikaris, D., Desirelli, A., Fabbricatore, P., Farinon, S., Feyzi, F., Gelebart, J., Gerwig, H., Girod, J., Grillet, J., Greenler, L., Gregerson, G., Herve, A., Horvath, I., Kaftanov, V., Coroller, A. L., Lesmond, C., Levesy, B., Lottin, J., Lottin, J., Loveless, R., Lyraud, C., Mason, W., Maugain, J., Musenich, R., Passardi, G., Pes, C., Petiot, P., Pintus, R., Pippin, J., Pogorelko, O., Priano, C., Rey, J., Rondeaux, F., Rousse, J., Smith, R., de Visser, T., Veillet, L., Wands, B., Waurick, G. 1997. CMS, the magnet project: Technical design report. *Journal of Physics: Conference Series*, p. 22–34.
- Agostinelli, S., Allison, J., Amako, K., Apostolakis, J., Araujo, H., Arce, P., Asai, M., Axen, D., Banerjee, S., Barrand, G., Behner, F., Bellagamba, L., Boudreau, J., Broglia, L., Brunengo, A., Burkhardt, H., Chauvie, S., Chuma, J., Chytracek, R., Cooperman, G., Cosmo, G., Degtyarenko, P., Dell'Acqua, A., Depaola, G., Dietrich, D., Enami, R., Feliciello, A., Ferguson, C., Fesefeldt, H., Folger, G., Foppiano, F., Forti, A., Garelli, S., Giani, S., Giannitrapani, R., Gibin, D., Cadenas, J. G., Gonzalez, I., Abril, G. G., Greeniaus, L., Greiner, W., Grichine, V. 2003. GEANT4: A Simulation toolkit. *Nucl. Instrum. Meth.*, A506: 250–303.
- Airapetian, A., Grabsky, V., Hakopian, H., Vartapetian, A., Fares, F., Moorhead, G. F., Sevier, M., Taylor, G., U.), S. T. M., Alexiev, D., Donnelly, I., Varvell, K., M.L. Williams (ANSTO, M., Hashemi-Nezhad, R., Peak, L., Saavedra, A., U.), J. U. S., Girtler, P., Kiener, C., Kneringer, E., Kuhn, D., U.), G. R. I., Abdinov, O., Aliev, F., Khalilzade, F., Mehdiyev, R. R., Rzaev, H., Usubov, Z. 1996. ATLAS calorimeter performance Technical Design Report, CERN.

Alam, M. 2005. Construction, Assembly and test of the ATLAS electromagnetic barrel calorimeter. *Nucl. Instrum. Methods A*, 034(388): 5–13.

Alam, M., Athar, S. B., Ling, Z., H. A., Mahmood, Severini, H. S., Timm, S. C., Wappler, F. R. 1998. ATLAS pixel detector: Technical design report.

Altarelli, G., Melé, B., Rückl, R. 1984. Chapter XIV: Physics of ep collisions in the TeV energy range. Physics of ep collisions in the TeV energy range. , (CERN-TH-3932): 20 p.

Amaldi, U. 2015. *Particle Accelerators: From Big Bang Physics to Hadron Therapy*. 1 edn. Springer International Publishing.

Arai, Y., Ball, B., Beretta, M., Boterenbrood, H., Brandenburg, G. W., Ceradini, F., Chapman, J. W., Dai, T., Ferretti, C., Fries, T., Gregory, J., da Costa, J. G., Harder, S., Hazen, E., Huth, J., Jansweijer, P. P. M., Kirsch, L. E., König, A. C., Lanza, A., Mikenberg, G., Oliver, J., Posch, C., Richter, R., Riegler, W., Spiriti, E., Taylor, F. E., Vermeulen, J. C., Wadsworth, B., Wijnen, T. A. M. 2008. ATLAS Muon Drift Tube Electronics. *Journal of Instrumentation*, 3(09): P09001.

Arratia Munoz, M. I. 2016. Studies of radiation damage in silicon sensors and a measurement of the inelastic proton–proton cross-section at 13 TeV. PhD thesis. Cambridge U.

Azzurri, P. 2006. The CMS Silicon Strip Tracker. *Journal of Physics: Conference Series*, 41(1): 127.

Baranov, S., Bosman, M., Dawson, I., Hedberg, V., Nisati, A., Shupe, M. 2005. Estimation of Radiation Background, Impact on Detectors, Activation and Shielding Optimization in ATLAS.

Bogacz, A., Latina, A., Pellegrini, D., Schulte, D. 2015. LHeC ERL Design and Beam-Dynamics Issues. In Proceedings, 6th ICFA Advanced Beam Dynamics Workshop on Energy Recovery Linacs (ERL 2015): Stony Brook, NY, USA, June 7-12, 2015. p. TU-IBLH2026.

Borrello, L., Messineo, A., Focardi, E., Macchiolo, A. 2003. Sensor Design for the CMS Silicon Strip Tracker.

Brun, R., Rademakers, F. 1997. ROOT: An object oriented data analysis framework. *Nucl. Instrum. Meth.*, A389: 81–86.

Brüning, O. 2013. Overview of the LHeC Design Study at CERN. In Proceedings, 4th International Particle Accelerator Conference (IPAC 2013): Shanghai, China, May 12-17, 2013. p. MOZB201.

Buchanan, N. J., Chen, L., Gingrich, D. M., Liu, S., Chen, H., Damazio, D., Densing, F., Duffin, S., Farrell, J., Kandasamy, S., Kierstead, J., Lanni, F., Lissauer, D., Ma, H., Makowiecki, D., Muller, T., Radeka, V., Rescia, S., Ruggiero, R., Takai, H., Wolniewicz, K., Ghazlane, H., Houmada, A., Hervas, L., Hott, T., Wilkens, H. G., Ban, J., Boettcher, S., Brooijmans, G., Chi, C. Y., Caughron, S., Cooke, M., Copic, K., Dannheim, D., Gara, A., Haas, A., Katsanos, I., Parsons, J. A., Simion, S., Sippach,

W., Zhang, L., Zhou, N., Eckstein, P., Kobel, M., Ladygin, E., Auge, E., Bernier, R., Bouchel, M., Bozzone, A., Breton, D., de la Taille, C., Falleau, I., Fournier, D., Imbert, P., Martin-Chassard, G., Perus, A., Richer, J. P., Moreau, N. S., Serin, L., Tocut, V., Veillet, J.-J., Zerwas, D., Colas, J., Dumont-Dayot, N., Massol, N., Perrodo, P., Perrot, G., Wingerter-Seez, I., Escalier, M., Hubaut, F., Laforge, B., Dortz, O. L., Schwemling, P., Collot, J., Dzahini, D., Gallin-Martel, M. L., Martin, P., Cwienk, W. D., Fent, J., Kurchaninov, L., Citterio, M., Mazzanti, M., Tartarelli, F., Bansal, V., Boulahouache, C., Cleland, W., Liu, B., McDonald, J., Paolone, V., Rabel, J., Savinov, V., Zuk, G., Benslama, K., Borgeaud, P., de la Broïse, X., Delagnes, E., Coguie, A. L., Mansoulié, B., Pascual, J., Teiger, J., Dinkespiler, B., Liu, T., Stroynowski, R., Ye, J., Zarzhitsky, P., Grahn, K. J., Hansson, P., Lund-Jensen, B., Chu, M. L., Lee, S. C., Su, D. S., Teng, P. K., Braun, H. M. 2008. ATLAS liquid argon calorimeter front end electronics. *Journal of Instrumentation*, 3(09): P09003.

Burkhardt, H. 2012. LHeC ring-ring option. *ICFA Beam Dyn. Newslett.*, 58: 76–86.

CERN 2017. Cern, <https://home.cern/>-(date of access:06.09.2017).

Collaboration, C. 2010. Calibration of the CMS drift tube chambers and measurement of the drift velocity with cosmic rays. *Journal of Instrumentation*, 5(03): T03016.

Cruz-Alaniz, E., Newton, D., Tomás, R., Korostelev, M. 2015. Design of the large hadron electron collider interaction region. *Phys. Rev. ST Accel. Beams*, 18(11): 111001.

Daguin, J., Arndt, K., Bertl, W., Noite, J., Petagna, P., Postema, H., Tropea, P., Verlaat, B. 2012. Evaporative CO₂ cooling system for the upgrade of the CMS pixel detector at CERN. p. 723–731.

Dainton, J. B., Klein, M., Newman, P., Perez, E., Willeke, F. 2006. Deep inelastic electron-nucleon scattering at the LHC. *JINST*, 1: P10001.

Daquino, G. G., Corti, G., Folger, G. 2006. Background radiation studies at LHCb using GEANT4. *IEEE Trans. Nucl. Sci.*, 53: 2907–2915.

Egana-Ugrinovic, D. 2016. Current challenges in fundamental physics. PhD thesis. The State University of New Jersey.

Evans, L., Bryant, P. 2008. LHC Machine. *JINST*, 3: S08001.

Fabjan, C. W., Gianotti, F. 2003. Calorimetry for particle physics. *Rev. Mod. Phys.*, 75: 1243–1286.

Fernandez, J. L. A., Adolphsen, C., Akay, A., Aksakal, H., Albacete, J. L. 2012. A Large Hadron Electron Collider at CERN: Report on the Physics and Design Concepts for Machine and Detector. *J. Phys.*, G39: 075001.

Ferrari, A., Sala, P. R., Fasso, A., Ranft, J. 2005. FLUKA: A multi-particle transport code (Program version 2005).

FLUKA 2017. Fluka, <http://www.fluka.org/fluka.php>-(date of access:09.09.2017).

Gorringe, T. P., Hertzog, D. W. 2015. Precision Muon Physics. *Prog. Part. Nucl. Phys.*, 84: 73–123.

Green, D. 2005. *The Physics of Particle Detectors*. Cambridge Monographs on Particle Physics, Nuclear Physics and Cosmology. Cambridge University Press.

Gruppen, C., Shwartz, B. 2008. *Particle detectors*. 2 edn. Cambridge University Press.

Hadjiiska, R., Litov, L., Pavlov, B., Petkov, P., Dimitrov, A., Beernaert, K., Cimmino, A., Costantini, S., Garcia, G., Lellouch, J., Marinov, A., Ocampo, A., Strobbe, N., Thyssen, F., Tytgat, M., Verwilligen, P., Yazgan, E., Zaganidis, N., Aleksandrov, A., Genchev, V., Iaydjiev, P., Rodozov, M., Shopova, M., Sultanov, G., Ban, Y., Cai, J., Xue, Z., Ge, Y., Li, Q., Qian, S., Avila, C., Chaparro, L. F., Gomez, J. P., Moreno, B. G., Oliveros, A. F. O., Sanabria, J. C., Assran, Y., Sharma, A., Abbrescia, M., Colaleo, A., Pugliese, G., Loddo, F., Calabria, C., Maggi, M., Benussi, L., Bianco, S., Colafranceschi, S., Piccolo, D., Carrillo, C., Iorio, O., Buontempo, S., Paolucci, P., Vitulo, P., Berzano, U., Gabusi, M., Kang, M., Lee, K. S., Park, S. K., Shin, S., Kim, M. S., Seo, H., Goh, J., Choi, Y., Shoaib, M. 2013. Simulation of the CMS Resistive Plate Chambers. *Journal of Instrumentation*, 8(03): P03001.

HERA, C. 2006. Hera, <http://www.desy.de/>-(date of access:06.09.2017).

Hrynevich, A. 2017. Performance of the ATLAS Tile Calorimeter. *JINST*, 12(06): C06021.

Huhtinen, M. 1996. The Radiation environment at the CMS experiment at the LHC. PhD thesis. CERN.

Huhtinen, M., Aarnio, P. A. 1995. Neutron and photon fluxes and shielding alternatives for the CMS detector at LHC. *Nucl. Instrum. Meth.*, A363: 545–556.

Kaußen, G. 2008. Silicon strip detector qualification for the CMS experiment. PhD thesis. Aachen, Tech. Hochsch.

Kayl, M. 2010. Tracking Performance of the ATLAS Inner Detector and Observation of Known Hadrons. In Hadron collider physics. Proceedings, 22nd Conference, HCP 2010, Toronto, Canada, August 23-27, 2010.

Keil, E. 1997. Large Hadron Collider electron-proton Option. , (CERN-LHC-093): 13.

Klein, M. 2011. Design Concepts for the Large Hadron Electron Collider. *Conf. Proc.*, C110904: 1942–1944.

Klein, M., Yoshida, R. 2008. Collider Physics at HERA. *Prog. Part. Nucl. Phys.*, 61: 343–393.

Kostka, P., Polini, A., South, D. M. 2013. A new detector for deep inelastic physics. *PoS, EPS-HEP2013*: 098.

König, S. 2009. Upgrade of the CMS Pixel Detector. *Proceedings of Science*, 035(6): .

Körner, G.-E. 2017. Nupecc, <http://www.nupecc.org/>-(date of access:04.012.2017).

Lehrach, A. 2012. Polarized electron-nucleon collider ENC at FAIR. *ICFA Beam Dyn. Newslett.*, 58: 29–35.

Lindström, G. 2003. Radiation damage in silicon detectors. *Nuclear Instruments and Methods in Physics Research Section A: Accelerators, Spectrometers, Detectors and Associated Equipment*, 512(1): 30 – 43. Proceedings of the 9th European Symposium on Semiconductor Detectors: New Developments on Radiation Detectors.

Linnik, B., Bus, T., Deveaux, M., Doering, D., Kudejova, P., Wagner, F. M., Yazgili, A., Stroth, J. 2017. Radiation damage caused by cold neutrons in boron doped CMOS active pixel sensors. *JINST*, 12(05): C05011.

Mallows, S., Azhgirey, I., Bayshev, I., Bergstrom, I., Cooijmans, T., Dabrowski, A., Glögler, L., Guthoff, M., Kurochkin, I., Vincke, H., Tajeda, S. 2016. Monte carlo simulations of the radiation environment for the cms experiment. *Nuclear Instruments and Methods in Physics Research Section A: Accelerators, Spectrometers, Detectors and Associated Equipment*, 824(Supplement C): 30 – 32.

Moser, H.-G. 2009. Silicon detector systems in high energy physics. *Prog. Part. Nucl. Phys.*, 63: 186–237.

Nassiri, A., Chase, B., Craievich, P., Fabris, A., Frischholz, H., Jacob, J., Jensen, E., Jensen, M., Kustom, R., Pasquinelli, R. 2016. History and Technology Developments of Radio Frequency (RF) Systems for Particle Accelerators. *IEEE Trans. Nucl. Sci.*, 63(2): 707–750.

Newman, P. 2009. Deep Inelastic Scattering at the TeV Energy Scale and the LHeC Project. *Nucl. Phys. Proc. Suppl.*, 191: 307–319.

Paolucci, P. 2006. The CMS muon system. In Astroparticle, particle and space physics, detectors and medical physics applications. Proceedings, 9th Conference, Como, Italy, October 17-21, 2005. p. 605–615.

Perez, E., Rizvi, E. 2013. The Quark and Gluon Structure of the Proton. *Rept. Prog. Phys.*, 76: 046201.

Plehn, T. 2012. Lectures on LHC Physics. *Lect. Notes Phys.*, 844: 1–193.

Polini, A., Kostka, P., Wallny, R. 2012. The LHeC central detector. In Proceedings, 20th International Workshop on Deep-Inelastic Scattering and Related Subjects (DIS 2012): Bonn, Germany, March 26-30, 2012. p. 1065–1070.

Pythia 2013. pythia6, <https://pythia6.hepforge.org/>-(date of access:06.09.2017).

Rata, R., Barlow, R., Lee, S. 2016. FLUKA Simulations for Radiation Protection at 3 Different Facilities. In Proceedings, 7th International Particle Accelerator Conference (IPAC 2016): Busan, Korea, May 8-13, 2016. p. TUPOY018.

- Rossi, P. 2016.** Physics opportunity with an electron-ion collider. *Journal of Physics: Conference Series*, 770(1): 012041.
- Russenschuck, S., Holzer, B. J., Tomas, R., Zimmermann, F., Kirby, G., Milanese, A., Tommasini, D. 2012.** Challenges for the Magnet System of LHeC. *Conf. Proc.*, C1205201: 1996–1998.
- S Chatrchyan, G Hmayakyan, V. C. 1997.** *CMS the Compact Muon Solenoid Muon technical design report*. Journal of Physics G. Chapter 1, p. 9–14.
- Sjostrand, T., Mrenna, S., Skands, P. Z. 2006.** PYTHIA 6.4 Physics and Manual. *JHEP*, 05: 026.
- Staśto, A. M. 2011.** Physics opportunities at an electron–ion collider. *Journal of Physics G: Nuclear and Particle Physics*, 38(12): 124037.
- T.Böhlen, F. 2005.** *The FLUKA Code: Developments and Challenges for High Energy and Medical Applications*. CERN. GENEVA. CERN-2005-010, INFN TC 05/11.
- The CMS Collaboration, S., Chatrchyan, G., Hmayakyan, V., Khachatryan, A., Sirunyan 2008.** The cms experiment at the cern lhc. *Journal of Instrumentation*, 3(08): S08004.
- Thyssen, F. 2012.** Performance of the Resistive Plate Chambers in the CMS experiment. *Journal of Instrumentation*, 7(01): C01104.
- Tommasini, D., Buzio, M., Chritin, R. 2012.** Dipole Magnets for the LHeC Ring-Ring Option. *IEEE Trans. Appl. Supercond.*, 22(3): 4000203.
- Verdier, A. 1991.** An Optimized e - p insertion for LEP and LHC. *Conf. Proc.*, C910506: 156–158.
- von Holtey, G. 1992.** Simulations of photon background to LEP detectors at 90-GeV beam energy.
- Widl, E. 2008.** Global Alignment of the CMS Tracker. PhD thesis. Vienna, Tech. U.
- Wiese, U.-J. 2010.** *The Standard Model of Particle Physics*. Institute for Theoretical Physics, University of Bern.
- Wilkens, H. 2009.** The ATLAS Liquid Argon calorimeter: An overview. *Journal of Physics: Conference Series*, 160(1): 012043.
- Williams, J. G., Griffin, P. J., Kelly, J. G., Figueroa, J. T. 1994.** Estimation of 1-MeV equivalent neutron fluence from dosimetry responses without spectrum unfolding. *IEEE Transactions on Nuclear Science*, 41(6): 2147–2151.
- Yamamoto, Y., Makida, R., Ruber, Y., Doi, T., Haruyama, F., Haug, H., Kate, T. 2008.** The ATLAS central solenoid. *Nucl. Instrum. Meth.*, A584: 53–74.
- Zimmermann, F. 2012.** LHeC ERL/Linac-ring option. *ICFA Beam Dyn. Newslett.*, 58: 86–100.

Zimmermann, F. 2013. ERL-Based Lepton-Hadron Colliders: eRHIC and LHeC. In Proceedings, 26th International Linear Accelerator Conference (LINAC12): Tel Aviv, Israel, September 9-14, 2012. p. TH3A03.



CURRICULUM VITAE

Name Last Name : Abdullah Nayaz
Place and Date of Birth : Wardak, Afghanistan – 05.03.1990
Language : Persian, English, Turkish, Urdu
Contact : abnayaz1@gmail.com

Educational Background

(Institution and Year):

High School : Helmand High School 2004-2008
University : Bamyan University, Physics
Department 2008-2013
Graduate School : Uludağ University
Graduate School of Natural and Applied Science
Department of Physics - 2017

Publication:

Nayaz, A., Piliçer E., Joya, M. 2017. Simulation of Radiation Environment for the LHeC Detector. *AIP Conf. Proc.*, (1815,060016-1–060016-4).

Research and Presentations:

Nayaz, A., Piliçer E. Simulation of Detector Response for the LHeC (poster presentation), International Workshop on Accelerators and detectors, 31 May–03 June 2016, Boğaziçi University, ISTANBUL, TURKEY.

Nayaz, A., Piliçer E., Joya, M. Simulation of Radiation Environment for the LHeC Detector presentation. Turkish Physical Society 32nd International Physics Congress (TPS32), 6–9 September 2016, BODRUM, TURKEY.

Nayaz, A., Piliçer E. Simulation of Radiation Environment for the LHeC Detector presentation. Congress of Young Physicists (Genç Fizikçiler Kongresi), 12–14 Oct. 2016, EGE University, IZMIR, TURKEY.

Nayaz, A., Kind, O. M. Muon Lifetime Measurements studies. Department of Physics, Homboldt University of Berlin, Oct.2016–Jan.2017, BERLIN, GERMANY.

